JEM Journal of Experimental Medicine

ARTICLE

Loss of decay-accelerating factor triggers podocyte injury and glomerulosclerosis

Andrea Angeletti[1,2*], Chiara Cantarelli[1,3*], Astgik Petrosyan[4,5*], Sofia Andrighetto[1,6], Kelly Budge[1], Vivette D. D'Agati[7], Susan Hartzell[1], Deborah Malvi[8], Chiara Donadei[1,9], Joshua M. Thurman[10], Danica Galešić-Ljubanović[11], John Cijiang He[1], Wenzhen Xiao[1], Kirk N. Campbell[1], Jenny Wong[1], Clara Fischman[1], Joaquin Manrique[12], Gianluigi Zaza[6], Enrico Fiaccadori[3], Gaetano La Manna[9], Miguel Fribourg[1], Jeremy Leventhal[1], Stefano Da Sacco[4,5], Laura Perin[4,5], Peter S. Heeger[1**], and Paolo Cravedi[1**]

Kidney glomerulosclerosis commonly progresses to end-stage kidney failure, but pathogenic mechanisms are still poorly understood. Here, we show that podocyte expression of decay-accelerating factor (DAF/CD55), a complement C3 convertase regulator, crucially controls disease in murine models of adriamycin (ADR)-induced focal and segmental glomerulosclerosis (FSGS) and streptozotocin (STZ)-induced diabetic glomerulosclerosis. ADR induces enzymatic cleavage of DAF from podocyte surfaces, leading to complement activation. C3 deficiency or prevention of C3a receptor (C3aR) signaling abrogates disease despite DAF deficiency, confirming complement dependence. Mechanistic studies show that C3a/C3aR ligations on podocytes initiate an autocrine IL-1β/IL-1R1 signaling loop that reduces nephrin expression, causing actin cytoskeleton rearrangement. Uncoupling IL-1β/IL-1R1 signaling prevents disease, providing a causal link. Glomeruli of patients with FSGS lack DAF and stain positive for C3d, and urinary C3a positively correlates with the degree of proteinuria. Together, our data indicate that the development and progression of glomerulosclerosis involve loss of podocyte DAF, triggering local, complement-dependent, IL-1β–induced podocyte injury, potentially identifying new therapeutic targets.

Introduction

Primary focal and segmental glomerulosclerosis (FSGS) is one of the leading causes of idiopathic nephrotic syndrome in adults (Kitiyakara et al., 2004). Available treatments achieve sustained remission in <50% of affected individuals, and the majority of those who do not achieve remission progress to end-stage renal disease (Cravedi et al., 2013a). This limited therapeutic efficacy and the associated significant toxicities of existing therapies for FSGS underscore a crucial unmet medical need for improved treatment approaches, ideally derived from new knowledge of disease pathogenesis.

While the discovery of genetic variants (Pollak, 2002) that predispose to the development of FSGS has provided some mechanistic insights into the pathogenesis of disease in a subset of patients, evidence derived from multiple experimental models strongly implicates podocyte injury and depletion as common pathogenic features of disease progression (Asano et al., 2005; Matsusaka et al., 2005; Wharram et al., 2005). The driving forces underlying podocyte injury remain inadequately understood, limiting progress in the development of novel therapeutics (Wharram et al., 2005).

The complement cascade, traditionally considered a constituent of innate immunity required for host defense against pathogens, is now recognized as a crucial pathogenic mediator of various kidney diseases (Cravedi and Heeger, 2014). Complement components produced by the liver and circulating in the plasma undergo activation through the classical and/or mannose-binding lectin pathways to mediate autoantibody-initiated glomerulonephritides (Mathern and Heeger, 2015). The alternative pathway of complement activation has been

[1]Department of Medicine, Icahn School of Medicine at Mount Sinai, New York, NY; [2]Division of Nephrology, Dialysis, Transplantation, Giannina Gaslini Children's Hospital, Genoa, Italy; [3]Dipartimento di Medicina e Chirurgia Università di Parma, UO Nefrologia, Azienda Ospedaliera-Universitaria Parma, Parma, Italy; [4]GOFARR Laboratory for Organ Regenerative Research and Cell Therapeutics in Urology, Children's Hospital Los Angeles, Los Angeles, CA; [5]Division of Urology, Saban Research Institute, University of Southern California, Los Angeles, CA; [6]Renal Unit, Department of Medicine, University Hospital of Verona, Verona, Italy; [7]Department of Pathology, College of Physicians and Surgeons, Columbia University, New York, NY; [8]"F. Addarii" Institute of Oncology and Transplantation Pathology, Bologna University, Bologna, Italy; [9]Dipartimento di Medicina Specialistica, Diagnostica e Sperimentale (DIMES), Policlinico Sant'Orsola-Malpighi, Bologna, Italy; [10]Department of Medicine, University of Colorado School of Medicine, Aurora, CO; [11]Department of Pathology, University of Zagreb School of Medicine, Zagreb, Croatia; [12]Nephrology Service, Complejo Hospitalario de Navarra, Pamplona, Spain.

*A. Angeletti, C. Cantarelli, and A. Petrosyan contributed equally to this paper; **P.S. Heeger and P. Cravedi are co–senior authors of this paper; Correspondence to Paolo Cravedi: paolo.cravedi@mssm.edu.

implicated in non–antibody-mediated models of glomerulonephritides, including murine and human C3 nephropathies (Servais et al., 2012; Sethi et al., 2012; Smith et al., 2019). While selected studies in murine models that mimic features of human FSGS have been associated with complement deposition, mechanisms linking complement to podocyte injury and FSGS remain poorly understood (Mathern and Heeger, 2015).

Decay-accelerating factor (DAF/CD55) is a glycophosphatidylinositol (GPI)-anchored protein that regulates complement activation on the surfaces on which it is expressed by accelerating the decay and inhibiting the reformation of surface-bound C3 convertases, together restraining amplification of the cascade (Medof et al., 1984). DAF has previously been shown to limit the phenotypic expression of kidney disease in several murine models (Bao et al., 2009) and is highly expressed on podocytes (Duann et al., 2019), raising the intriguing hypothesis that podocyte-expressed DAF crucially and locally restrains complement-dependent podocyte injury that results in glomerulosclerosis.

In the present study, by using human immortalized podocytes and mice conditionally lacking DAF or C3a receptor (C3aR) on podocytes, we show that, upon adriamycin (ADR) injection, DAF is enzymatically cleaved, leading to complement activation and formation of C3a. C3a/C3aR signaling on podocytes promotes IL-1β production that, in an autocrine fashion, induces podocyte cytoskeleton rearrangement and loss, leading to glomerulosclerosis. We found that the same mechanism is operative in streptozotocin (STZ)-induced diabetic kidney disease in mice and also in humans with FSGS.

Results

ADR-induced FSGS associates with reduced DAF expression and complement activation in BALB/c mice

We initially analyzed glomerular patterns of DAF expression in naive BALB/c mice kidneys (a strain known to be susceptible to ADR [Wang et al., 2000]) by immunofluorescence (IF). We observed strong DAF staining that colocalized with synaptopodin, indicative of podocyte expression in naive animals (Fig. 1 A). 1 wk after ADR administration, we observed markedly decreased glomerular DAF expression (Fig. 1, B and C), accompanied by glomerular C3b deposition (Fig. 1, D–F), the latter consistent with DAF's physiological function of restraining local complement activation (Medof et al., 1984).

To begin testing for functional links between DAF expression and ADR-induced kidney disease, we injected ADR into male and female WT or germline DAF$^{-/-}$ BALB/c mice. These experiments showed significantly more albuminuria (Fig. 1 G) with more severe histological changes (Fig. 1 H) in the DAF-deficient BALB/c mice, regardless of sex (Fig. 1 I), noting that females are more resistant to ADR-initiated glomerular injury, consistent with previous reports and with human studies (Chen et al., 1998; Garovic and August, 2016; Sakemi et al., 1996).

Genetically determined DAF absence confers ADR susceptibility in B6 mice

We next investigated the relationship between DAF expression and FSGS in C57BL/6 (B6) mice, a strain that is resistant to the development of ADR-induced FSGS lesions (Papeta et al., 2010). Whereas the glomeruli of naive B6 mice costained for DAF and synaptopodin similarly to those in BALB/c mice (Fig. S1 A), ADR administration did not reduce glomerular DAF expression in B6 mice (Fig. S1, B and C). ADR administration modestly but significantly increased glomerular C3b deposition in the B6 mice (Fig. S1, D–F).

While ADR administration did not induce proteinuria or glomerulosclerosis in WT B6 mice (verifying previous work [Papeta et al., 2010; Zheng et al., 2006; Zheng et al., 2005]), ADR remarkably induced proteinuria and glomerulosclerosis or tubular atrophy/interstitial sclerosis in congenic B6 DAF$^{-/-}$ mice (Fig. 1, J–M), associated with increased glomerular C3b deposition (Fig. S1, G–I). Because DAF has complement-independent functions, including being a ligand of the transmembrane receptor CD97 and a host receptor for infection by the malaria parasite (Dho et al., 2018), we performed additional control studies to verify that ADR-induced FSGS in DAF-deficient mice is complement dependent (Fig. 1, J–M). ADR administration to DAF$^{-/-}$C3$^{-/-}$ mice indeed did not result in proteinuria, glomerulosclerosis, or tubular sclerosis.

Podocyte-specific DAF-null mice are more susceptible to ADR

DAF is an intrinsic complement regulator that limits complement activation only on the cells on which it is expressed (Medof et al., 1987), raising the possibility that DAF expression specifically on podocytes locally regulates the ADR-induced, complement-dependent podocyte injury in this model. To test this, we newly generated B6 DAF$^{fl/fl}$ mice and crossed them to podocin-Cre^{POS} animals (Fig. S2 A) and confirmed selective absence of DAF from podocyte surfaces (but detection on tubular cells) in these DAF$^{fl/fl}$ podocin-Cre^{POS} mice (Fig. S2, B–E). DAF$^{fl/fl}$ podocin-Cre^{POS} mice are healthy without growth abnormalities and do not spontaneously develop proteinuria, renal insufficiency, or other renal functional abnormalities when followed for up to 12 mo of age (data not shown). Whereas ADR injection did not induce proteinuria or glomerulosclerosis in the DAF$^{fl/fl}$ podocin-Cre^{NEG} control animals (similar to WT B6; Fig. 2, A and B), ADR administration to DAF$^{fl/fl}$ podocin-Cre^{POS} animals resulted in albuminuria by day 21 along with histological evidence of glomerulosclerosis and tubular atrophy/interstitial sclerosis, the latter similar in severity to the lesions in germline DAF$^{-/-}$ mice (Fig. 2, A, C, E, and F). As an additional control, we also generated DAF$^{fl/fl}$ CD11c-Cre^{POS} mice that lack DAF on myeloid immune cells. In these animals, ADR injection did not induce proteinuria or glomerulosclerosis and tubular atrophy/interstitial sclerosis, a result that did not differ from the ADR-injected DAF$^{fl/fl}$ podocin-Cre^{NEG} control animals (Fig. 2, A, B, and D–F). At 35 d after ADR injection, ultrastructural analysis showed no abnormalities in vehicle-injected animals, but ADR resulted in significantly higher podocyte foot process effacement in DAF$^{fl/fl}$ podocin-Cre^{POS} animals versus podocin-Cre^{NEG} control animals (Fig. 2, G and H). Together the data newly support the conclusion that podocyte-expressed DAF is protective in this model system.

To provide insight into the complement-dependent mechanisms that result in glomerular injury in the absence of DAF, we stained kidneys from DAF$^{fl/fl}$ podocin-Cre^{NEG} and podocin-Cre^{POS}

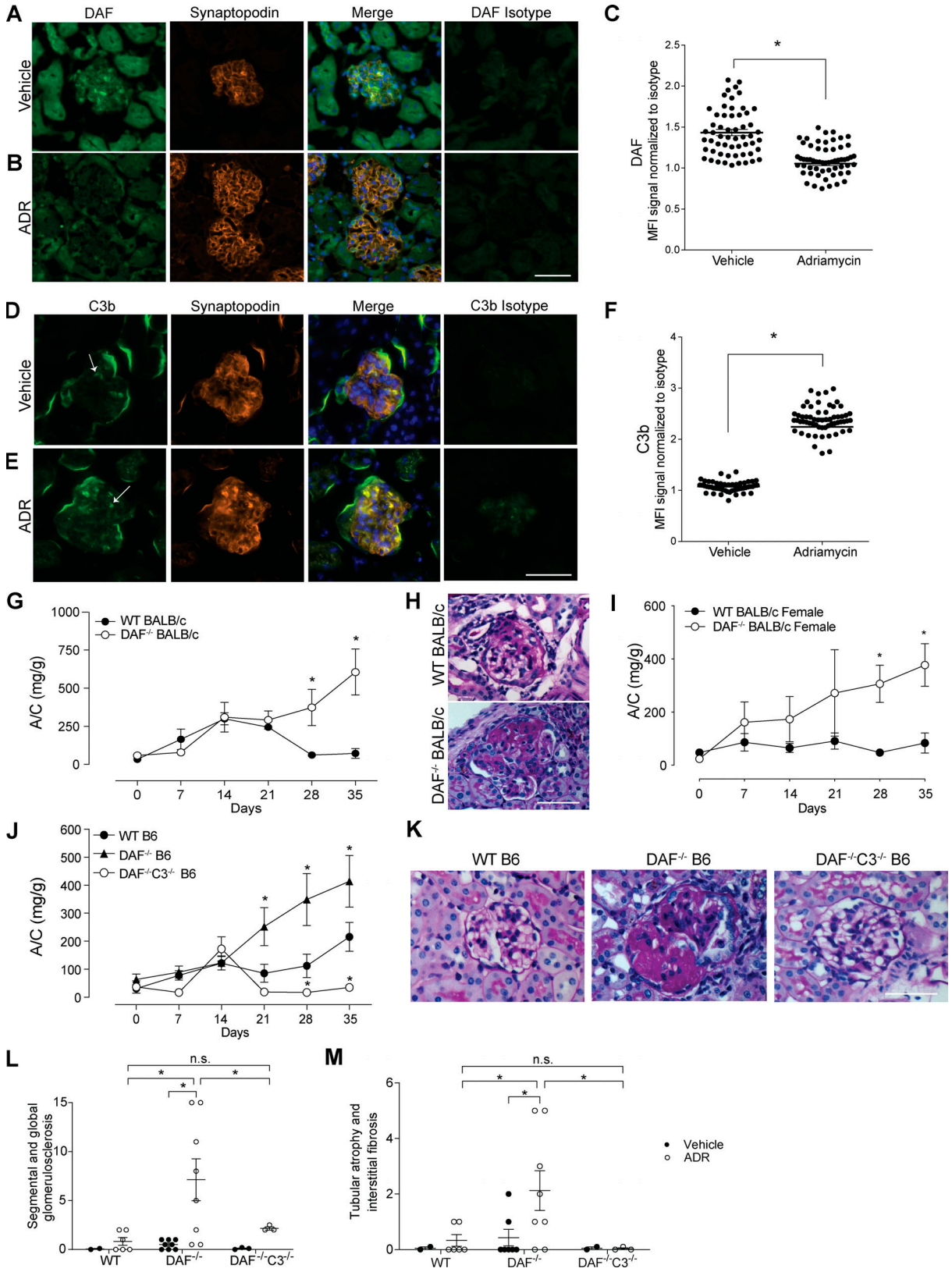

Figure 1. **Glomerular DAF downregulation promotes murine ADR-induced FSGS through a complement-mediated mechanism. (A–F)** Representative pictures and data quantification of glomerular (A–C) DAF and (D–F) C3b staining of male WT BALB/c mice treated with vehicle or ADR (10 mg/kg, i.v.). Background staining for C3b is present in the periphery of all glomeruli, with higher intraglomerular C3b staining (arrows) in the ADR-treated animals. DAF and C3b glomerular fluorescence intensity was quantified relative to isotype using ImageJ software. At least 30 glomeruli per mouse from two animals were included in the analysis. Each dot represents a glomerulus. **(G and H)** Urinary A/C at weekly intervals (G) and representative renal histological (PAS stain)

lesions (H) of male WT (n = 8) or DAF$^{-/-}$ (n = 9) BALB/c mice sacrificed at 5 wk after ADR injection (10 mg/kg, i.v.). **(I)** Urinary A/C at weekly intervals of female WT (n = 5) or DAF$^{-/-}$ (n = 4) BALB/c mice sacrificed at 5 wk after ADR injection (10 mg/kg, i.v.). **(J–M)** Urinary A/C at weekly intervals (J) and representative renal histological (PAS) lesions (K) with data quantification (L and M) of male WT (n = 18), DAF$^{-/-}$ (n = 13), or DAF$^{-/-}$C3$^{-/-}$ (n = 4) B6 mice sacrificed at 5 wk after ADR injection (20 mg/kg, i.v.). All experimental data were verified in at least three independent experiments. *P < 0.05 versus WT at the same time point. n.s., not significant. Scale bars: 50 µm. Error bars are SEM.

mice after ADR injection for complement activation products. These analyses showed increased glomerular deposition of C3b, without C1q or C4b in DAF$^{fl/fl}$ podocin-Cre^{POS} compared with podocin-Cre^{NEG} control animals (Fig. S2, F–J), implicating complement activation predominantly via the alternative pathway.

Phenotypic expression of FSGS requires C3aR

Building on (1) the above data (Fig. 1; Fig. 2, A–C; Fig. S1; and Fig. S2, B–E), (2) DAF's known mechanism of restraining complement activation at the C3 convertase step, and (3) our previous reports that DAF deficiency augments C3a production (Cravedi and Heeger, 2014; Cravedi et al., 2013b), we postulated that, in the absence of DAF, locally produced C3a ligates podocyte-expressed C3aR to function as a crucial driver of the podocyte injury in this model. After documenting that podocytes express C3aR and that C3aR expression is increased 2 wk after ADR injection (Fig. S3, A–C), we administered ADR to groups of germline DAF$^{-/-}$C3aR$^{-/-}$ mice and to WT and DAF$^{-/-}$ control animals (Fig. 2, I and J). These experiments showed that germline C3aR deficiency fully prevented the ADR-induced FSGS observed in DAF-deficient mice. We observed similar protection against FSGS development in ADR-administered BALB/c mice treated with the selective C3aR antagonist (C3aR-A) SB290157 (1 mg/kg/d s.c. for 28 d by injection pumps; Fig. 2, K and L). C3aR-A administration to ADR-treated BALB/c mice also showed significantly less albuminuria than untreated control animals after ADR injection (albumin/creatinine [A/C], 253 ± 59 versus 752 ± 97 mg/g; P < 0.05). When we administered ADR to B6 DAF$^{fl/fl}$ podocin-Cre^{POS} with or without C3aR-A, we also observed a significant decrease in the clinical and histological manifestations of kidney disease (Fig. 2, M and N).

ADR promotes phospholipase D–mediated cleavage of DAF from podocyte surfaces

Our data thus far indicate that ADR-induced DAF downregulation on podocytes contributes to the development of glomerulosclerosis. To discern the molecular mechanisms underlying this ADR-induced decrease in DAF expression, we quantified *Daf* mRNA (qPCR) in kidneys from BALB/c mice treated with vehicle or ADR. These experiments surprisingly showed significantly more *Daf* gene expression after ADR injection (3.9 ± 2.1-fold versus 1.1 ± 0.4-fold, respectively; P < 0.05; n = 3 animals per group), despite the above observed decrease in glomerular DAF by IF staining. In vitro cultures of immortalized human podocytes (hiPod) with or without ADR similarly showed that ADR augmented *Daf* gene expression (2.3 ± 0.1-fold versus 1.0 ± 0.1-fold, respectively; P < 0.01; n = 3 experiments per group), but they showed decreased DAF on cell surfaces (Fig. 3, A and B).

DAF is a GPI-anchored membrane protein that can be cleaved by phospholipases, including, among others, phospholipase D (PLAD), raising the possibility that ADR-induced DAF surface protein downregulation is mediated by PLAD-dependent GPI cleavage. We observed increased *Gpld1* gene expression in the kidneys from BALB/c mice 1 wk after ADR treatment compared with saline injection (4.4 ± 1.0-fold versus 1.0 ± 0.2-fold, respectively; P < 0.05) and in hiPod exposed to ADR compared with vehicle-treated cells for 24 h (2.0 ± 0.6-fold versus 1.0 ± 0.1-fold, respectively; P < 0.05). Immunoblots of hiPod showed a significant increase in PLAD protein following ADR exposure (Fig. 3, C and D). To test for a causal link between PLAD expression and DAF cleavage, we exposed podocytes to ADR in the presence or absence of a selective PLAD inhibitor (PLADi). Consistent with the hypothesis that ADR promotes DAF cleavage by increasing PLAD expression, the PLADi preserved membrane expression of DAF in podocytes exposed to ADR (Fig. 3, A and B). Addition of the PLADi also reduced soluble DAF in the supernatants of podocytes exposed to ADR, supporting the hypothesis that PLAD reduces DAF expression through GPI cleavage (Fig. 3, E and F). When we tested the urine of WT BALB/c mice 2 wk after injection with ADR or vehicle control, we found cleaved DAF in ADR-treated animals (but not in control animals), further supporting the conclusion that ADR induces glomerular DAF cleavage in vivo (Fig. 3 G).

DAF-deficient mice are more susceptible to STZ-induced diabetic kidney disease

To test the hypothesis that DAF cleavage and associated complement activation modulate clinical and histological expression of another form of glomerulosclerosis, we studied mice with STZ-induced type 1 diabetic kidney disease, which is manifested pathologically by increased mesangial expansion and sclerosed glomeruli (Breyer et al., 2005). In this model, STZ associated with glomerular deposition of C3b (Fig. 4, A and B). Whereas WT BALB/c mice 20 wk after STZ show modest albuminuria and glomerular lesions (Fig. 4, C and D), STZ-treated DAF$^{-/-}$ mice show significantly higher urinary albumin (Fig. 4 C) and more severe glomerular changes (Fig. 4 D), despite similar levels of hyperglycemia between groups (Fig. 4 E). STZ-treated B6 DAF$^{fl/fl}$ podocin-Cre^{POS} mice lacking DAF on podocytes had higher levels of C3b deposition in the glomeruli than control animals (Fig. 4, F and G), which was associated with more severe diabetic kidney disease (Fig. 4, H and I) despite similar glycemic levels (Fig. 4 J). Together the findings newly implicate DAF deficiency specifically on podocytes and resultant complement activation as contributing to the pathogenesis of this form of glomerulosclerosis as well as to FSGS.

DAF and complement in human FSGS and diabetic kidney disease

To test whether the above murine findings potentially apply to humans with FSGS and diabetic kidney disease, we examined data from one large published RNA-sequencing study using

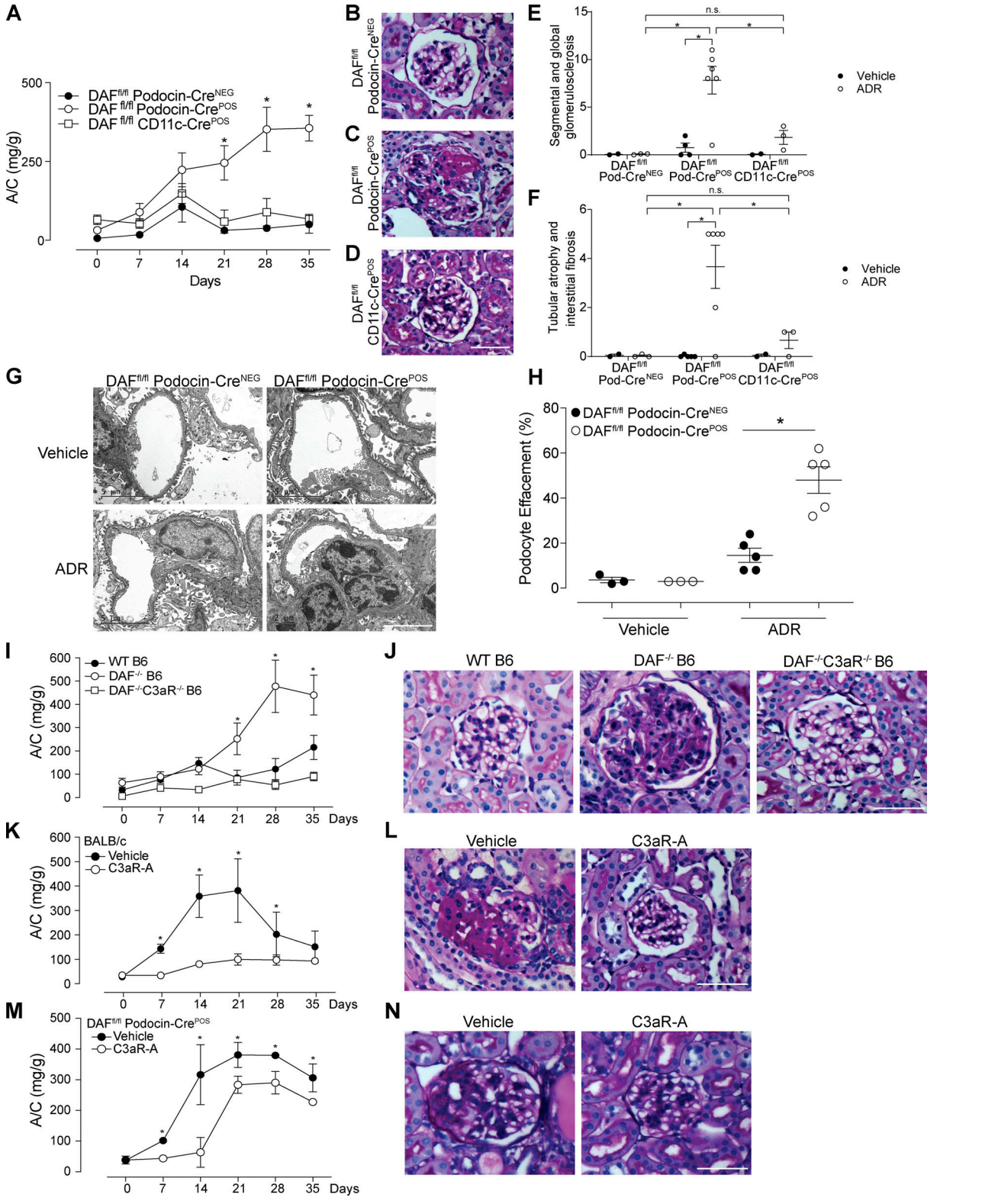

Figure 2. **Podocyte-specific removal of DAF from podocytes increases susceptibility to ADR-induced injury through C3a/C3aR signaling. (A–F)** Urinary A/C at weekly intervals (A) and representative renal histological (PAS) lesions (B–D) with data quantification (E and F) of male DAF$^{fl/fl}$ podocin-Cre^{NEG} (n = 10), DAF$^{fl/fl}$ podocin-Cre^{POS} (n = 19), and DAF$^{fl/fl}$ CD11c-Cre^{POS} (n = 5) mice injected with ADR (20 mg/kg, i.v.) and sacrificed after 5 wk. **(G and H)** Representative electron micrographs (G) and quantification (H) of podocyte effacement in 8-wk-old DAF$^{fl/fl}$ podocin-Cre^{POS} or DAF$^{fl/fl}$ podocin-Cre^{NEG} mice at 5 wk after treatment with saline or ADR (20 mg/kg, i.v.). **(I and J)** Urinary A/C at weekly intervals (I) and representative renal histological (PAS) lesions (J) of WT (n = 16), DAF$^{-/-}$ (n = 13), and DAF$^{-/-}$C3aR$^{-/-}$ (n = 4) male B6 mice injected with ADR (20 mg/kg, i.v.). **(K and L)** Urinary A/C at weekly intervals (K) and representative renal histological (PAS) lesions (L) of male BALB/c mice given ADR (10 mg/kg, i.v.) and treated with C3aR-A (1 mg/kg/d, s.c.; n = 5) or

saline (n = 5). **(M and N)** Urinary A/C at weekly intervals (M) and representative renal histological (PAS) lesions (N) of male B6 DAF$^{fl/fl}$ podocin-Cre^{POS} mice given ADR (20 mg/kg, i.v.) and treated with C3aR-A (1 mg/kg/d, s.c.; n = 5) or saline (n = 5). *P < 0.05 versus podocin-Cre^{NEG}, WT, or C3aR-A. All experimental data were verified in at least three independent experiments. n.s., not significant. Scale bars: 50 µm. Error bars are SEM.

Nephroseq (http://www.nephroseq.org/). The study compared expression levels of RNA extracted from microdissected glomerular samples from patients with FSGS (n = 17), diabetic nephropathy (n = 12), and control individuals (kidney living donors; n = 35; Ju et al., 2013). Our analyses showed significantly increased expression of mRNA for *C3*, *C3aR*, and *C5aR* in samples from patients with FSGS or diabetic kidney disease compared with control individuals (Fig. 5, A–C), providing associative evidence that the complement system is implicated in the pathogenesis of human diseases. In the same FSGS and diabetic kidney disease patients, we also observed increased *DAF* mRNA expression in the diseased kidneys versus control individuals (Fig. 5 D). When we stained kidney biopsies from 18 patients with FSGS, we observed increased C3d deposition compared with control individuals (Fig. 5, E and F; Table 1). Consistent with murine data (Fig. 1, A–C), DAF staining of glomeruli with FSGS (n = 18) showed weaker expression than control kidneys (n = 10; Fig. 5, G and H). As one approach to test whether the lower DAF expression results in complement activation in the kidney, we quantified urinary C3a and proteinuria in urine samples from 27 patients with FSGS and in 10 healthy control individuals (Fig. 5, I–L; Table 2). These analyses showed a significant correlation between urinary C3a and proteinuria at the time of diagnosis in the FSGS cohort (Fig. 5 I), while no C3a was detected in the urine of healthy control individuals. We observed that the elevations in proteinuria and urinary C3a were

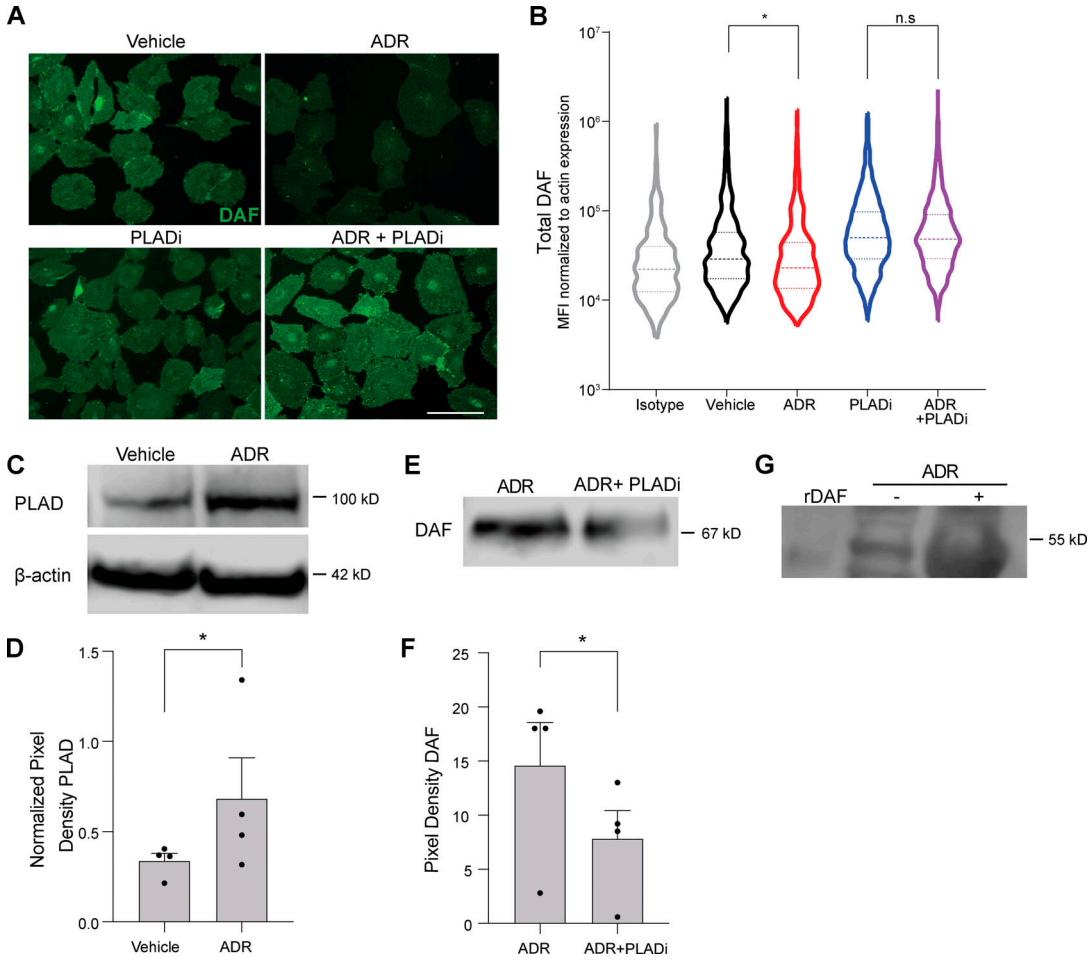

Figure 3. **ADR induces PLAD-dependent cleavage of DAF. (A and B)** Representative images (A) and distribution of DAF expression (B) quantified in hiPod exposed to vehicle, ADR (0.3 µg/ml), PLADi (1 µM), or ADR + PLADi (0.3 µg/ml in 1 µM) for 24 h. DAF IF signal was normalized to actin expression pixel by pixel, and the MFI for each cell was computed. Results are representative of two independent experiments with similar results. **(C and D)** Representative blots (C) and densitometric analysis (D) of PLAD expression in hiPod cell lysates previously exposed to vehicle or ADR for 24 h. **(E and F)** Representative blots (E) and densitometric analysis (F) of DAF in the supernatants of hiPod exposed to ADR for 24 h with or without PLADi (WB). **(G)** Representative blot of DAF in the urine from BALB/c male mice at 2 wk after treatment with vehicle or ADR compared with recombinant mouse DAF (rDAF). In each group, we pooled and concentrated urine samples from eight mice (see Materials and methods). All experimental data were verified in at least three independent experiments. *P < 0.05; n.s., not significant. Scale bars: 50 µm. Error bars are SEM.

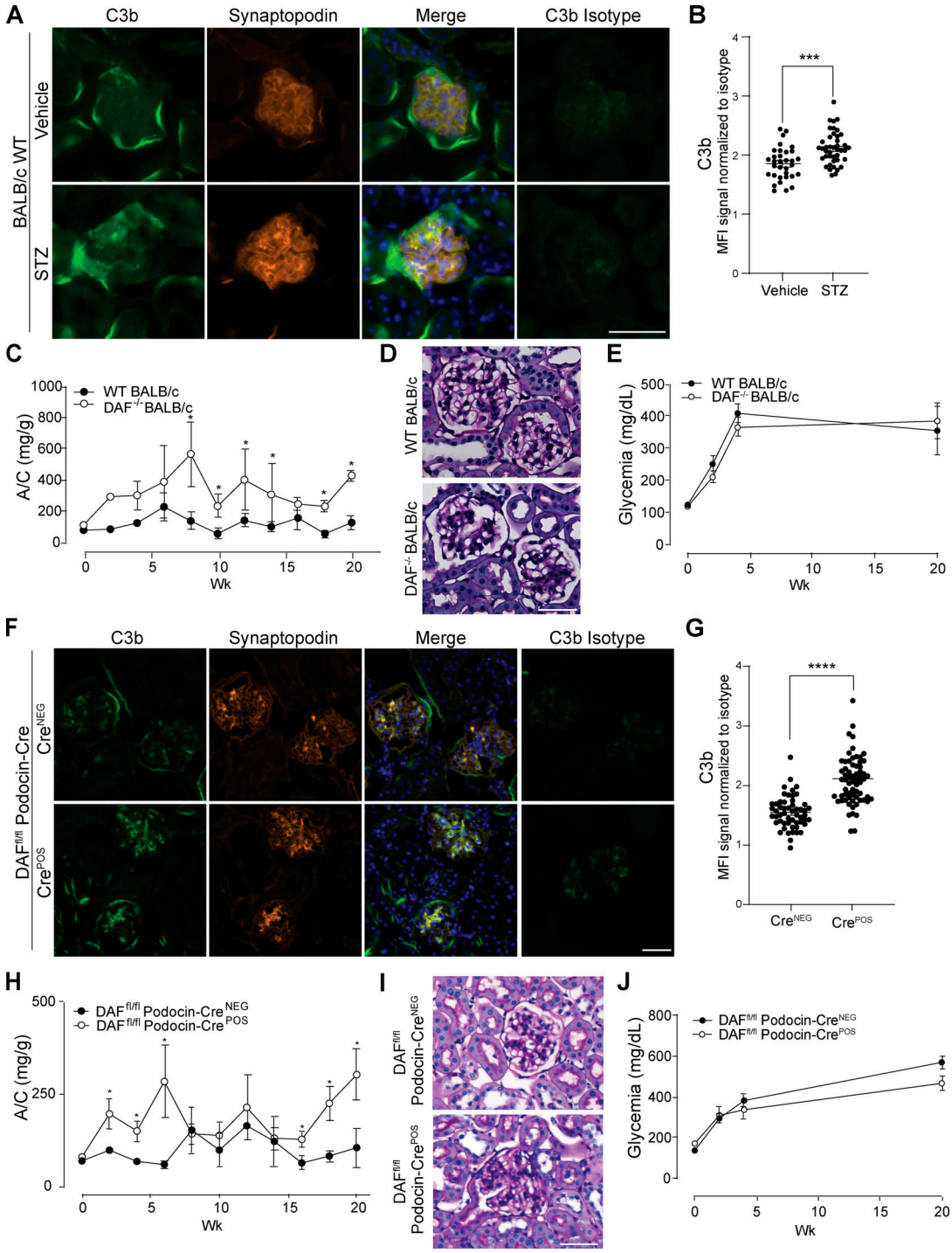

Figure 4. **Glomerular DAF downregulation promotes murine STZ-induced diabetic kidney disease. (A and B)** Representative pictures (A) and data quantification (B) of glomerular C3b in BALB/c WT mice at 5 wk after vehicle or STZ injection. ***P < 0.001. **(C and D)** Urinary A/C at weekly intervals (C) and representative renal histological (PAS) lesions (D) of male WT (n = 8) or DAF$^{-/-}$ (n = 5) BALB/c mice sacrificed at 5 wk after STZ injection (50 mg/kg, i.p., for five consecutive days). *P < 0.05 versus WT at the same time point. **(E)** Glycemic levels of mice injected with STZ shown in A–D. **(F and G)** Representative pictures (F) and data quantification (G) of glomerular C3b in DAF$^{fl/fl}$ podocin-Cre$^{NEG/POS}$ B6 mice at 5 wk after STZ injection. ****P < 0.001. **(H and I)** Urinary A/C at weekly intervals (H) and representative renal histological (PAS) lesions (I) of male DAF$^{fl/fl}$ podocin-Cre^{NEG} (n = 9) or podocin-Cre^{POS} (n = 8) B6 mice sacrificed at 20 wk after STZ injection (50 mg/kg, i.p., for five consecutive days). *P < 0.05 versus DAF$^{fl/fl}$ podocin-Cre^{NEG} at the same time point. **(J)** Glycemic levels of mice injected with STZ shown in H and I. Only mice that reached glycemia >300 mg/dl at 2 wk after STZ injection were included in this set of experiments. All experimental data were verified in at least three independent experiments. Scale bars: 50 µm. Error bars are SEM.

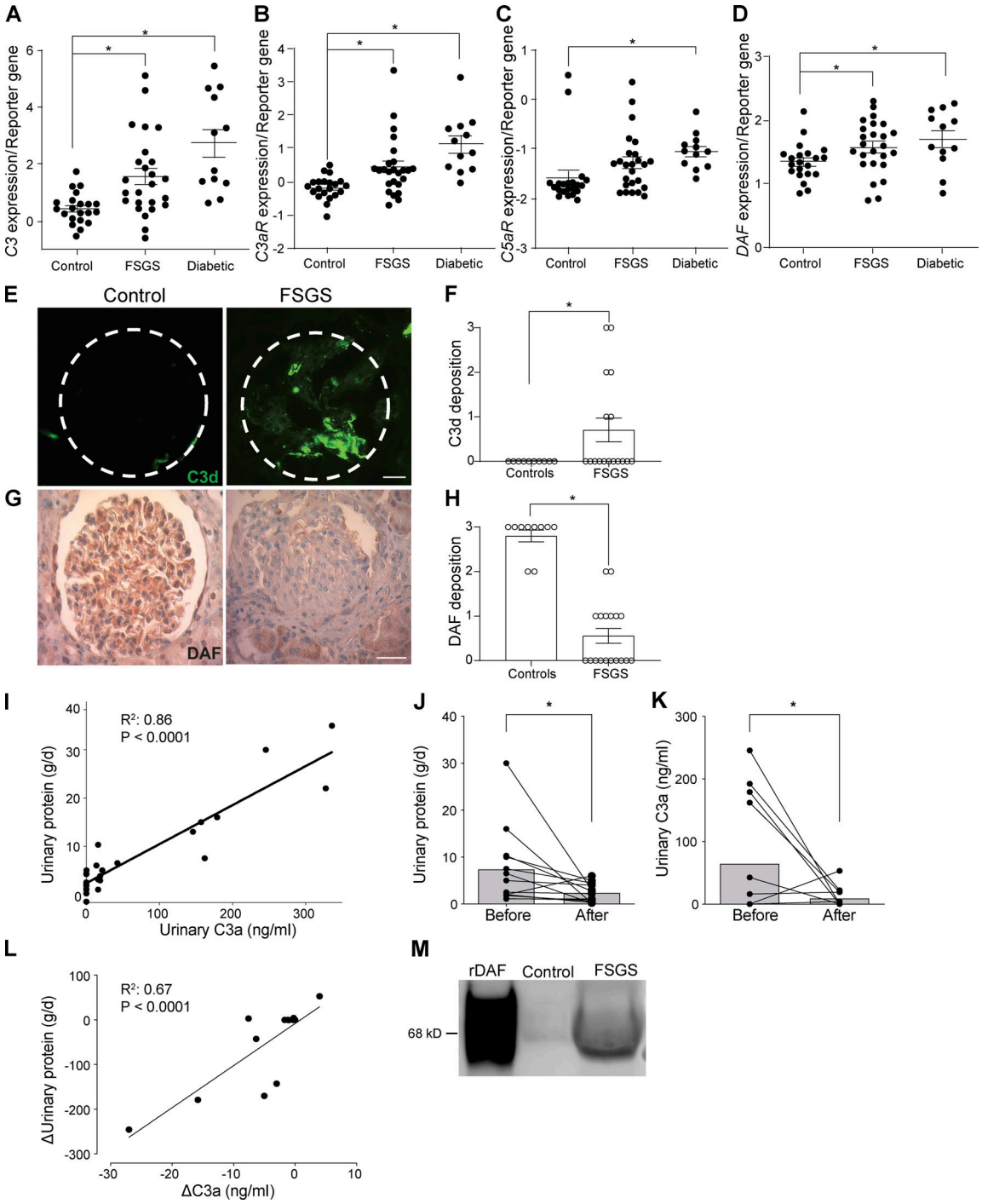

Figure 5. **FSGS in humans is associated with DAF down-regulation and complement activation. (A–D)** *C3* (A), *C3aR* (B), *C5aR* (C), and *DAF* mRNA (D) expression in glomeruli of human biopsy specimens with pathological diagnosis of FSGS or diabetic kidney disease compared with normal kidneys. Data are from previously published microarray studies by Ju et al. (2013) and were subjected to further analysis using Nephroseq. **(E–H)** Representative renal staining and data quantification for C3d (IF; E and F) and DAF (immunohistochemistry; G and H) in patients with FSGS (n = 18) and in kidneys from healthy renal donors (n = 10). **(I)** Correlation between protein and C3a in urine samples from 27 patients with FSGS taken at the time of kidney biopsy (before therapy). **(J and K)** Differences in proteinuria (J) and urinary C3a (K) measured before versus 3–6 mo after steroid therapy in a subset of 13 patients with FSGS. **(L)** Correlation between the change in proteinuria and change in urinary C3a before and after therapy for each of the same 13 patients. **(M)** Representative blot of DAF in the urine from healthy control individuals and patients with FSGS compared with recombinant human DAF (rDAF). In each group, we pooled and concentrated urine samples from five and five subjects, respectively (see Materials and methods). *P ≤ 0.05. Scale bars: 25 µm. Error bars are SEM.

Table 1. **Baseline characteristics of individuals included in Fig. 5, E–H**

	Patients with FSGS	Healthy controls
Sex	14 M/4 F	4 F/6 M
Age, yr	47.8 ± 14.4	69 ± 9
Ethnicity		
Caucasian	16	10
African American	2	0
Serum creatinine, mg/dl	1.6 ± 1.0	0.9 ± 0.2
Serum albumin, g/dl	2.9 ± 0.8	4.1 ± 0.7
Proteinuria, g/24 h	6.4 ± 6.5	n.d.

Data are expressed as numbers or average ± SD. F, female; M, male; n.d., not determined.

significantly reduced after therapy (Fig. 5, J and K), and their changes correlated with one another (Fig. 5 L). Together with previous observations by others (Lenderink et al., 2007; Thurman et al., 2015; Turnberg et al., 2006), our data support the concept that complement components are present in the urinary space of subjects with proteinuria and are activated by DAF down-regulation, leading to the formation of C3a and C5a.

We also tested for cleaved DAF in the urine of patients with FSGS and healthy control individuals by immunoblotting. These assays showed that soluble/cleaved DAF was detectable in the urine of patients with FSGS but not in healthy control individuals, further supporting the concept that DAF reduction observed in patients with FSGS is due to its cleavage (Fig. 5 M).

C3a/C3aR signaling promotes actin cytoskeleton rearrangement in human podocytes

Absence of surface DAF lifts restraint on local complement activation, resulting in production of C3a (Cravedi et al., 2013b; Heeger et al., 2005; Raedler et al., 2009; Sheen et al., 2017). As our above data (Fig. 2, I–N) showed that C3aR signaling on podocytes drives ADR-induced FSGS, we next tested molecular links between C3a/C3aR and podocyte injury. After verifying that cultured hiPod express C3aR (Fig. S3, D and E), we exposed them to recombinant C3a for 24 h and used IF to quantify actin cytoskeleton expression and distribution because they are functionally linked to podocyte structure and permselectivity (Macconi et al., 2006). C3a induced rearrangement of actin cytoskeleton (Fig. 6, A and B), an effect that was prevented by the selective C3aR antagonist SB290157 but not vehicle control (Fig. 6, A and B), implicating C3aR as the mediator of C3a effects. To test for the effect of C3a on podocyte viability, we stained the cells for caspase-3 (apoptotic marker), and we showed that C3a–C3aR interaction promotes cell apoptosis as well (Fig. 6 C). We similarly observed C3a/C3aR-induced cytoskeleton rearrangement of human podocytes derived from amniotic fluid kidney progenitor cells (Da Sacco et al., 2013; Da Sacco et al., 2010; Petrosyan et al., 2019; Fig. 6, D and E).

Table 2. **Baseline characteristics of patients included in Fig. 5, I–L**

	Patients with FSGS	Healthy controls
Sex	11 F/16 M	3 F/7 M
Age, yr	39.9 ± 14.2	40.1 ± 7.1
Ethnicity		
Caucasian	24	10
Asian	3	0
Serum creatinine, mg/dl	1.9 ± 1.9	n.d.
Serum albumin, g/dl	3.0 ± 0.6	n.d.
Proteinuria, g/24 h	5.2 ± 3.1	n.d.

Data are expressed as numbers or average ± SD. F, female; M, male; n.d., not determined.

Data from studies performed in both human and mouse podocytes show that podocyte damage (including damage caused by C3a/C3aR1 signaling) increases expression of Snail that, in turn, decreases nephrin expression and disrupts the slit diaphragm (Li et al., 2014; Matsui et al., 2007; Wu and Dedhar, 2001; Zhao et al., 2016). In accordance with these observations by others, addition of C3a increased podocyte Snail and TGF-β protein expression in cultured human podocytes, and the effects were prevented by addition of a C3aR antagonist (Fig. 6, F and G).

To provide additional mechanistic insight, we used a protein array to measure changes in 105 cytokines and mediators of kidney injury from supernatants of hiPod exposed to vehicle, C3a, or C3a plus C3aR-A for 24 h. These analyses showed that C3a selectively increased 16 of the molecules in the array (Fig. 6 H). We used the Genome-scale Integrated Analysis of Gene Networks in Tissues (GIANT, now HumanBase) Bayesian integration (Wong et al., 2018) to capture the most relevant podocyte-specific functional interactions between C3aR and nephrin, a major component of the slit diaphragm. Each interaction (or functional relationship) in the networks generated represents a body of data, probabilistically weighted and integrated, focused on a particular biological question/tissue. Of the 16 molecules selectively upregulated by C3a (but not by C3a + C3aR-A) the GIANT analyses indicated that IL-1β provided the strongest predicted functional connection between C3aR and nephrin selectively in podocytes (Fig. 6 I).

C3a/C3aR signaling is linked to podocyte injury and FSGS through IL-1β

IL-1β is a proinflammatory cytokine produced by monocytes, lymphocytes, and other cells, including podocytes (Anders, 2016; Yan et al., 2018), and it is detected in glomeruli of subjects with proteinuric nephropathies, including FSGS (Niemir et al., 1997). IL-1β is produced as a precursor (pro–IL-1β) that must be cleaved by the multiprotein inflammasome complex in order to be activated and secreted (Sutterwala et al., 2014). Given that C3a/C3aR ligations transduce signals that promote IL-1β release in other cell types, including monocytes (Asgari et al., 2013; Haeffner-Cavaillon et al., 1987), we hypothesized that C3a/C3aR signaling promotes podocyte production and release of IL-1β, which in turn binds to IL-1β receptor (IL-1R1) on the same cells (paracrine and autocrine) to promote nephrin reduction (Takano

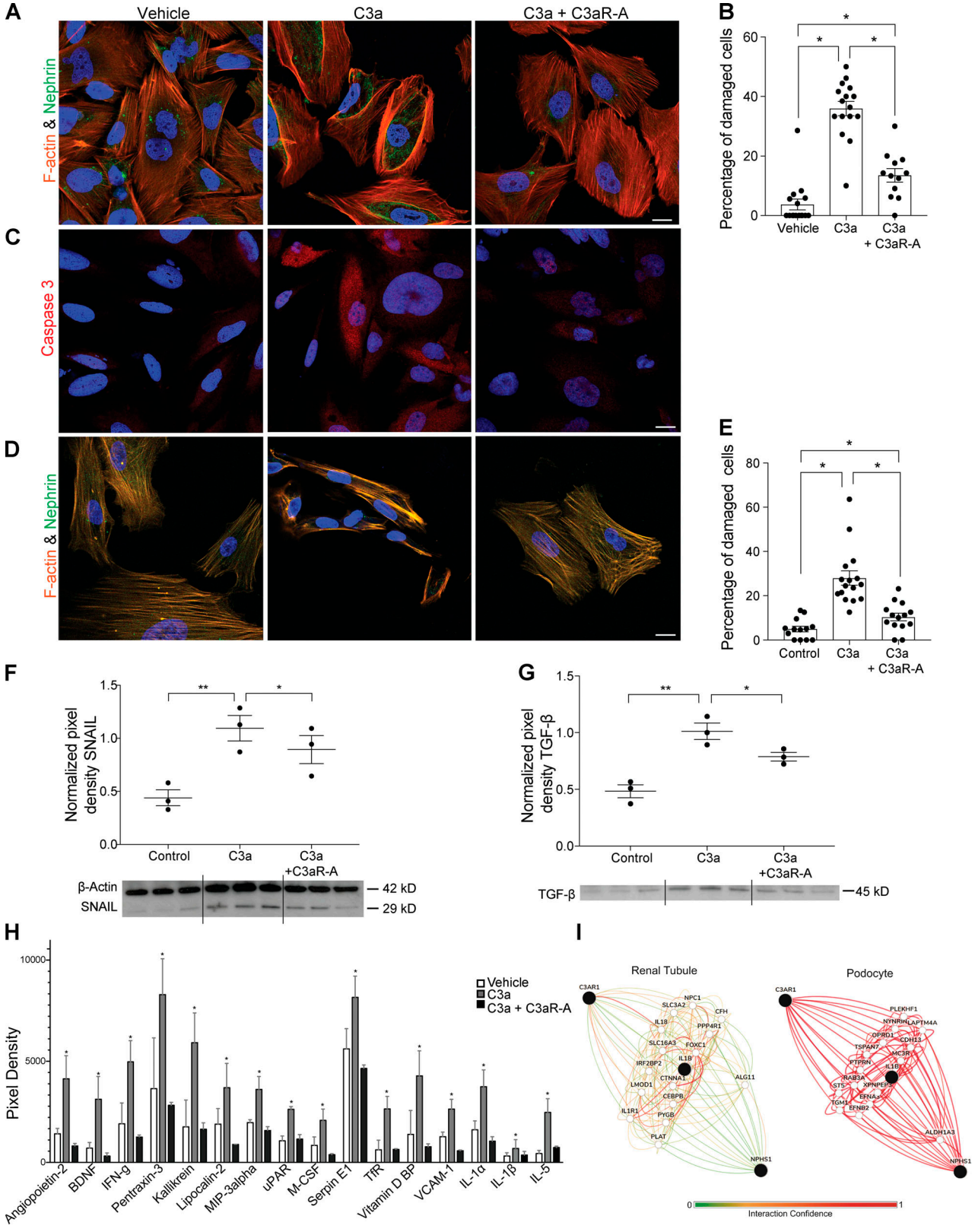

Figure 6. **C3a–C3aR interaction disrupts actin cytoskeleton in human cultured podocytes. (A and B)** Representative images (A) and quantification (B) of cell injury of hiPod exposed to vehicle, C3a (50 nM), or C3a + C3aR-A (50 nM) for 24 h and stained for F-actin and nephrin. **(C)** Representative images of caspase-3 staining of the same cells pictured above. **(D and E)** Representative images (D) and quantification (E) of cell injury of amniotic fluid–derived human podocytes exposed to vehicle, C3a (50 nM), or C3a + C3aR-A (50 nM) for 24 h and stained for F-actin and nephrin. *P < 0.05. **(F and G)** Representative blots and densitometric analysis of Snail (F) and TGF-β (G) expression in hiPod treated with vehicle, C3a, or C3a + C3aR-A for 24 h. Snail was measured in cell lysates; TGF-β was measured in cell supernatants. *P < 0.05; **P < 0.01. **(H)** Differentially expressed proteins in the supernatants of hiPod exposed for 24 h to vehicle,

C3a (50 nM), or C3a + C3aR-A (50 nM; Proteome Profiler Human XL Cytokine Array). The cytokines represented here are the only ones among the 105 analyzed (see Materials and methods) whose expression levels significantly differed in C3a-treated podocytes versus both vehicle- and C3a + C3aR antagonist–treated cells. *P < 0.05 versus vehicle and C3a + C3aR antagonist. **(I)** Functional network showing the relationship between C3aR, IL-1β, and nephrin in renal tubular cells and in podocytes (https://hb.flatironinstitute.org/gene/; query genes *C3aR*, *IL1B*, and *NPHS1*; tissue, renal tubules or podocytes; maximum number of genes, 15). All experimental data were verified in at least two independent experiments. Scale bars: 20 µm. Error bars are SEM.

et al., 2007) and cytoskeleton rearrangement (Schlondorff, 2008). Consistent with our hypothesis, when we cultured hiPod with C3a, we observed a significant increase in *IL1B* transcripts (Fig. 7 A). When podocytes were cultured with LPS with or without C3a, we found that C3a significantly augmented IL-1β secretion (Fig. 7 B), the latter indicative of increased inflammasome activation (Asgari et al., 2013).

To test the hypothesis that C3a-induced IL-1β production is responsible for podocyte injury, we exposed hiPod to C3a, C3a + anti–IL-1β–neutralizing antibody, or isotype IgG alone (Fig. 7 C). These experiments showed that C3a reduced nephrin expression and that the effect was abolished when C3a was administered with anti–IL-1β–neutralizing antibody but not isotype control, together supporting the conclusion that C3a-induced reduction in nephrin requires IL-1β/IL-1R1 signaling as an intermediary step.

On the basis of evidence that IL-1β induces actin cytoskeleton rearrangement through IL-1R1 signaling in podocytes, we tested whether blockade of IL-1β prevents C3a-induced effects on the cytoskeleton. C3a promoted rearrangement of the podocyte cytoskeleton, and this effect was fully prevented when cells were exposed to C3a in conjunction with anti–IL-1β–neutralizing antibody (Fig. 7, D and E).

Finally, to test how the in vitro mechanisms implicating pathogenic links among C3aR, IL-1β, and podocyte dysfunction apply to the development of ADR-induced FSGS, we treated ADR-injected BALB/c mice with anti–IL-1β–neutralizing antibody or isotype control, beginning on the day of ADR injection. These experiments showed significantly lower albuminuria levels and reduced histological evidence of disease in mice treated with the neutralizing antibody (Fig. 8, A and B), despite

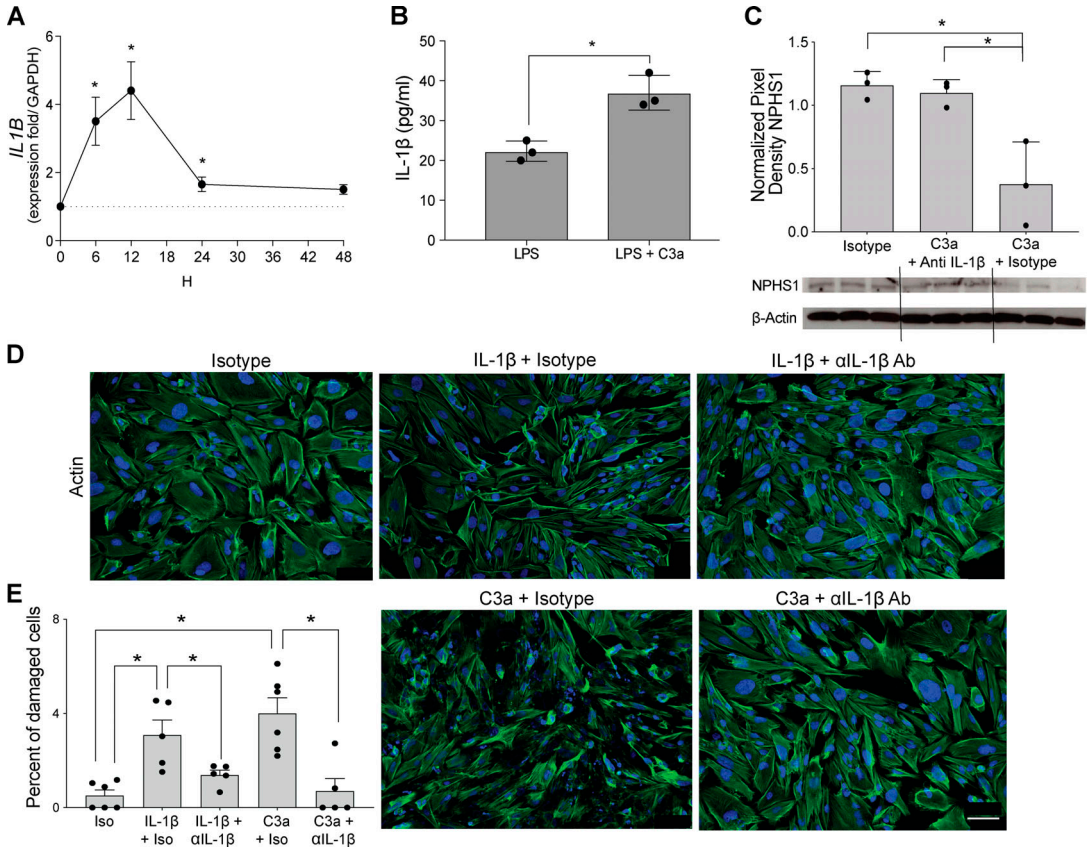

Figure 7. **IL-1β mediates complement-induced podocyte injury in vitro. (A)** *IL1B* gene expression in hiPod at serial time points after C3a stimulation (50 nM). **(B)** IL-1β levels in the supernatants of hiPod at 24 h after LPS (5 ng/ml) with or without C3a stimulation. **(C)** Nephrin expression in hiPod at 24 h after stimulation with isotype, C3a + anti–IL-1β–neutralizing antibody, and C3a + isotype (WB). *P < 0.05 versus 0 h. **(D and E)** Representative images (D) and quantification (E) of cell injury of hiPod exposed to isotype control, IL-1β (50 ng/ml) + isotype control, or IL-1β (50 ng/ml) + anti–IL-1β–neutralizing antibody (0.5 µg/ml; upper row). In the bottom row, the same cells were exposed to C3a + isotype control or C3a + anti–IL-1β–neutralizing antibody for 1 h. All experimental data were verified in at least two independent experiments. *P < 0.05. Scale bars: 100 µm. Error bars are SEM.

similar amounts of C3b deposited in the glomeruli (Fig. 8, C and D). To formally test whether these protective effects are due to IL-1R signaling, we administered ADR to DAF$^{fl/fl}$ podocin-Cre^{POS} and Cre^{NEG} littermate control animals and treated them with anakinra or vehicle control starting from the day of ADR administration. These experiments showed that IL-1R blockade with anakinra also prevented the onset of albuminuria and glomerular lesions (Fig. 8, E and F). Together with the previous experiments, the data indicate that DAF-regulated C3a/C3aR ligations on podocytes cause ADR-induced glomerular injury via an IL-1β–dependent mechanism. Data from Nephroseq analyses of glomeruli of patients with FSGS or healthy control individuals showed increased levels of *IL1B* and *IL1R1* mRNA levels in individuals with FSGS, supporting the conclusion that similar mechanisms apply to humans (Fig. 8, G and H).

Discussion

Individuals with FSGS commonly demonstrate C3d deposits in the glomeruli (Gephardt et al., 1986; Habib et al., 1988), indicative of complement activation, and the presence of C3d associates with worse clinical outcomes (Zhang et al., 2016); however, the mechanisms linking complement activation to FSGS have remained obscure. Our present results newly describe that DAF cleavage on podocytes lifts restraint on complement activation and pathogenically contributes to the clinical and histological expression of FSGS.

The experiments with conditional DAF removal from podocytes newly indicate that pathogenic complement activation occurs locally on the surface of these cells. The fact that C3aR deficiency in podocytes is also protective indicates that C3a–C3aR interaction is a major effector mechanism responsible for the complement-induced podocyte injury. Systemic administration of a C3aR antagonist prevents ADR-induced glomerulosclerosis despite DAF deficiency, providing a rationale for studies testing the hypothesis that pharmacological blockade of C3a formation or signaling downstream C3aR will prevent progression of FSGS in humans.

While we acknowledge that ADR does not promote FSGS in humans, ADR-induced FSGS is a widely accepted murine model of glomerulosclerosis that mimics the main histological and clinical features of the disease, including foot process effacement and podocyte loss (Papeta et al., 2010; Pippin et al., 2009; Yang et al., 2018). Our data with conditional DAF-knockout mice were replicated in male and female BALB/c mice, as well as in B6 animals that are more resistant to ADR. Previous data indicate that different susceptibility to ADR across mouse strains depends on mutations in the *Prkdc* gene, which encodes a critical nuclear DNA double-stranded break repair protein (Papeta et al., 2010). However, our data suggest that strain susceptibility to ADR could also depend at least in part on different predisposition to complement activation. While both BALB/c and B6 mice expressed DAF in podocytes, DAF cleavage and C3b deposition in the glomeruli were more pronounced in BALB/c animals. Overall, these data concur to document that complement activation is a central pathogenic mechanism in glomerulosclerosis affecting disease severity.

We also found that mice with STZ-induced diabetic kidney disease show C3b deposition in the glomeruli, which is increased by DAF removal from podocytes, along with disease severity. These murine data, along with evidence of complement activation in humans with diabetic kidney disease (Fig. 5, A–D; Bus et al., 2018; Flyvbjerg, 2017), support the concept that complement activation is implicated in the progressive glomerulosclerosis associated with multiple renal diseases.

Our in vitro and in vivo data newly indicate that ADR promotes DAF cleavage on podocyte membranes through the upregulation of PLAD. PLAD is specific for the GPI anchor found on many eukaryotic cell surface proteins, including DAF (Davitz et al., 1989). To the best of our knowledge, this is the first demonstration that PLAD is produced by human podocytes and regulates DAF expression on their surfaces. Development of small molecules with PLAD inhibitory activity may therefore have clinical utility in patients with FSGS (Frohman, 2015).

Our in vitro studies show that C3a–C3aR interaction in podocytes leads to significant cell cytoskeleton rearrangements and that this is mediated by C3a-induced increase in IL-1β production that, through autocrine and paracrine signaling, reduces nephrin expression. Though C3a has been shown to lead to increased IL-1β production in monocytes (Asgari et al., 2013) and podocytes are known for their capacity to make IL-1β (Anders, 2016), to the best of our knowledge, this is the first study reporting a link between C3a/C3aR signaling and IL-1β production in podocytes. Our experiments also show that, while C3a promotes *IL-1B* transcription in a TLR-independent fashion, C3a-induced increase in fully mature IL-1β required TLR signaling by LPS. Importantly, our data indicate that treatment with anakinra prevents ADR-induced glomerulosclerosis, while data by others showed that later treatment initiation was less effective (Boehm et al., 2019). Our new mechanistic insights linking DAF downregulation to glomerulosclerosis through C3aR-dependent IL-1β production and subsequent IL-1R signaling provide a potential explanation to account for the documented anti-proteinuric effects of anti–IL-1β antibody treatment in individuals with glomerular injury from amyloidosis (Dinarello et al., 2012; Varan et al., 2019).

Our data have been confirmed in both male and female animals, and our in vitro and in vivo data in mice are corroborated by human findings, implicating a role for complement in both murine and human FSGS. In renal biopsies from patients with FSGS, we found that C3d deposition in the glomeruli was paralleled by a reduction in DAF expression, suggesting that complement activation is at least in part mediated by downregulation of this regulator. The increased *DAF* gene expression in the glomeruli from patients with FSGS might represent a compensatory mechanism in response to decreased DAF surface expression by cleavage, potentially secondary to increased C3a production and C3a/C3aR signaling. This association between urinary C3a and proteinuria further supports a pathogenic role for alternative pathway complement activation in the disease and the testable hypothesis that C3a represents also a biomarker for disease activity more sensitive than proteinuria.

C5aR is also expressed in podocytes and upregulated after ADR injection (Fig. S3, F–H), and it could contribute to disease

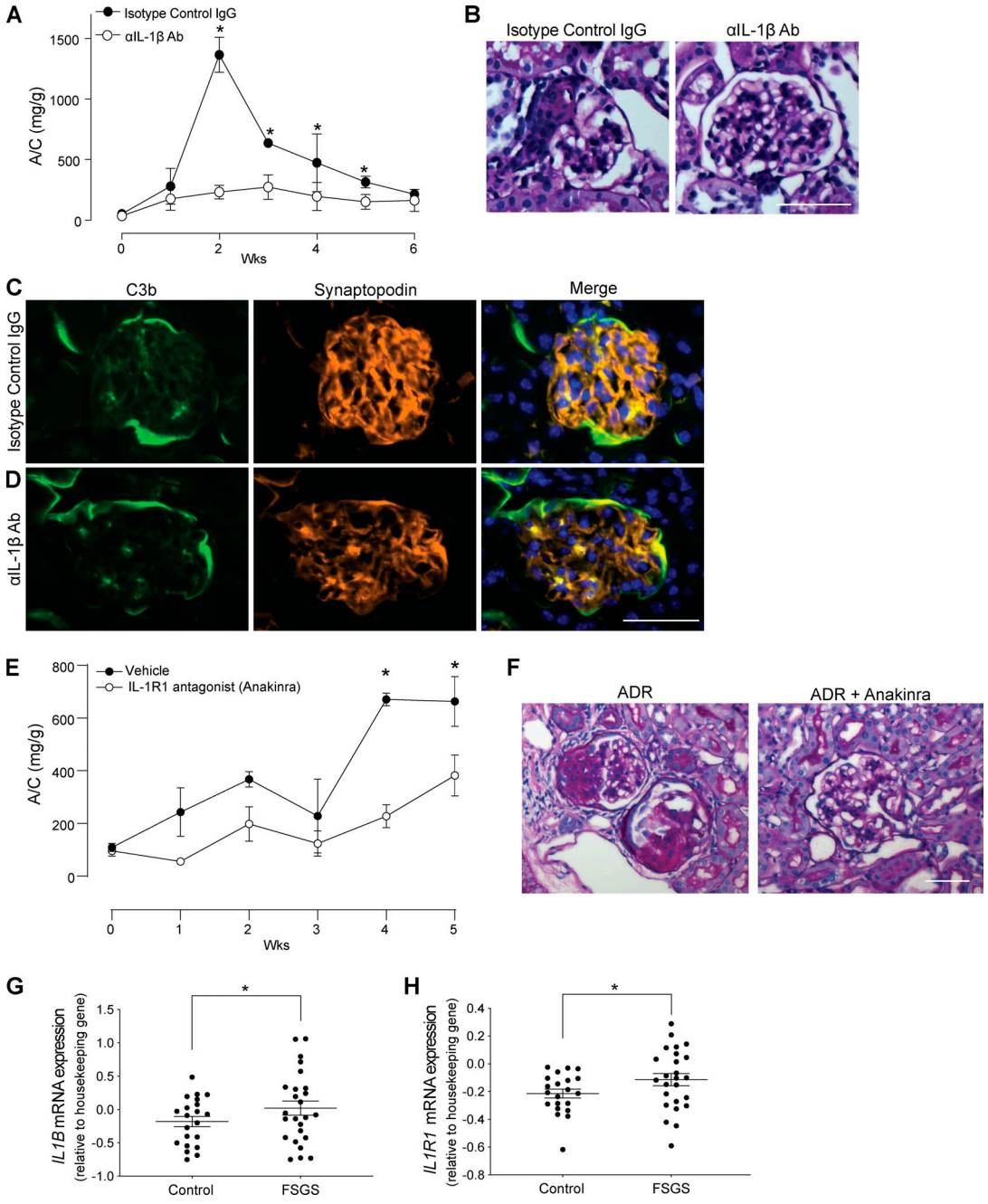

Figure 8. **IL-1β mediates complement-induced podocyte injury in vivo. (A and B)** Urinary A/C (A) and representative renal histological changes (B) in BALB/c mice injected with 10 mg/kg of ADR (i.v.) and rat anti-mouse IL-1β–neutralizing mAb (50 µg/mice twice per week, i.p.; *n* = 4) or isotype control (*n* = 4). Scale bars: 50 µm. *P < 0.05 versus anti–IL-1β–neutralizing antibody at the same time point. **(C and D)** Representative images of C3b deposition in the glomeruli of mice treated with (C) anti–IL-1β–neutralizing antibody or (D) isotype control. **(E and F)** Urinary A/C (E) and representative renal histological changes (F) in B6 $DAF^{fl/fl}$ podocin-Cre^{POS} male mice injected with 10 mg/kg of ADR (i.v.) and anakinra (25 mg/kg/d through s.c. pumps; *n* = 4) or vehicle control (*n* = 3). Scale bars: 50 µm. *P < 0.05 versus anakinra at the same time point. **(G and H)** *IL1B* (G) and *IL1R1* mRNA expression (H) in glomeruli of human biopsy specimens with pathological diagnosis of FSGS compared with normal kidneys. Data are from previously published microarray studies by Ju et al. (2013) and were subjected to further analysis using Nephroseq. *P < 0.05. All experimental data were verified in at least two independent experiments. Error bars are SEM.

expression. While we did not specifically test the effects of C5aR signaling in our model systems, the fact that genetic or pharmacological blockade of C3aR almost fully prevents disease severity induced by the absence of DAF suggests that C3aR signaling is the dominant effect.

Our data suggest that podocyte-expressed DAF protects podocytes from spontaneous complement activation and provides an explanation to account for several previously unexplained observations made by others: (1) C3d deposition in the glomeruli of subjects with FSGS (Liu et al., 2017) or diabetic kidney disease

(Bus et al., 2018) correlates with poor renal survival, and (2) subjects with loss-of-function mutations in *CD55* gene (encoding for DAF) present evidence of glomerular injury (Angeletti et al., 2017; Kurolap et al., 2017; Ozen et al., 2017). Intriguingly, data from the early 1990s indicate that steroids, the most widely used first-line therapy for FSGS, inhibit activation of the alternative pathway of complement activation (Packard and Weiler, 1983). In light of our new discoveries, this effect could explain, at least in part, the antiproteinuric effects of steroid treatment in patients with FSGS.

While we did not formally determine the pathway through which complement activation was initiated in our studies, our documentation of glomerular C3b deposition without C1q nor C4b suggests a predominance of the alternative pathway. This interpretation is consistent with previously reported data by Lenderink et al. (2007) showing that mice lacking factor B, a regulator of alternative complement pathway activation, develop lower proteinuria than WT control animals upon ADR injection. Similarly, factor D–deficient mice show lower proteinuria and less glomerular and tubulointerstitial injury after ADR injection than WT animals (Turnberg et al., 2006). In a model of FSGS due to protein overload (Morigi et al., 2016), factor H–deficient mice displayed higher C3b glomerular deposition and more severe lesions than WT control animals, overall supporting a pathogenic role of alternative complement activation in FSGS.

In summary, our data support a conceptual shift regarding the specific role of DAF in the observed complement activation in FSGS and how C3a/C3aR signaling in podocytes contributes to the pathogenesis of FSGS, diabetic kidney disease, and possibly other proteinuric nephropathies. Various inhibitors of complement component C3 and antagonists of the C3aR, along with IL-1β or IL-1R1 antagonists (including the one employed in our present study) are actively being developed by pharmaceutical companies. Therefore, our data provide the foundation for future interventional trials testing the hypothesis that counteracting C3a/C3aR and/or IL-1β/IL-1R1 signaling prevents or retards progression of proteinuric nephropathies.

Materials and methods

Mice and procedures

WT BALB/c and C57BL/6J (B6), and MRL-*lpr* mice were purchased from The Jackson Laboratory. We intercrossed B6 Df1$^{-/-}$ mice (DAF$^{-/-}$; Heeger et al., 2005) with C3$^{-/-}$ mice (from The Jackson Laboratory) to produce DAF$^{-/-}$C3$^{-/-}$ animals or with C3aR1$^{-/-}$ mice (C3aR$^{-/-}$ from The Jackson Laboratory) to produce DAF$^{-/-}$C3aR$^{-/-}$ animals. We backcrossed the B6 DAF$^{-/-}$ animals 14 generations to BALB/c to produce BALB/c DAF$^{-/-}$ animals.

To generate DAF$^{fl/fl}$ mice, we obtained embryonic stem cells from the European Conditional Mouse Mutagenesis Program (EUCOMM), into which loxP sites were inserted flanking exons 3 and 4 of the *Cd55* (Daf1) gene. The embryonic stem cells were injected into pseudopregnant B6 mice (The Jackson Laboratory) by standard techniques at the Mouse Genetics and Gene Targeting CoRE facility at Icahn School of Medicine at Mount Sinai. Founders were validated by genotyping. We then crossed them to a flp/flp mouse (from The Jackson Laboratory) to remove the neocassette and then backcrossed to B6 and crossed with B6 mice expressing the podocin-Cre or CD11c-Cre (The Jackson Laboratory).

Animal experiments were performed with the approval of the Institutional Animal Care and Use Committee of Icahn School of Medicine at Mount Sinai in New York City. Male and female mice (aged 8–12 wk), with a body weight of 20–25 g, were treated with a single retroorbital injection of ADR (doxorubicin HCl; Ben Venue Laboratories) at the dose of 10 mg/kg for BALB/c or 20 mg/kg for B6 mice. Urinary A/C was measured weekly until sacrifice.

Diabetes mellitus was induced with intraperitoneal injection of STZ (Streptozocin; Sigma-Aldrich) at the dose of 50 mg/kg body weight for five consecutive days. Blood glucose and urinary A/C were measured every 2 wk, and all animals were sacrificed after 20 wk of the experiment. The animals were considered diabetic if their blood glucose levels reached 300 mg/dl or more.

C3aR-A (SB290157; Sigma-Aldrich) or vehicle control was administered through s.c. pumps (ALZET microosmotic pump, model 1004; DURECT Corp.) at the dose of 1 mg/kg/d (powder dissolved in PBS and 10% DMSO) for 28 d. Rat antimouse IL-1β mAb (*InVivo*Mab, B122; Bio X Cell) or isotype control (*InVivo*Mab polyclonal Armenian hamster IgG; Bio X Cell) was administered i.p. at the dose of 50 µg/mouse twice per week for 6 wk (Coffelt et al., 2015). Anakinra (Amgen) was administered through s.c. pumps (ALZET microosmotic pump, model 1004; DURECT Corp.) at the dose of 25 mg/kg/d for 28 d.

Renal histology

To obtain kidneys for histological analyses, mice were anesthetized with i.p. injection of 100 µl of a solution made of sterile ketamine (16 mg/ml) and xylazine (7 mg/ml) in Gibco PBS (Thermo Fisher Scientific) and transcardially perfused with periodate-lysin-paraformaldehyde fixate at 4% in PBS. Kidneys were harvested and frozen in optimal cutting temperature compound (Tissue-Tek O.C.T.; Sakura Finetek) or embedded in paraffin.

Light microscopy

Paraffin-embedded kidney sections (3 µm) were stained with periodic acid–Schiff (PAS). Histological scoring was performed in a blinded manner by a renal pathologist as previously described (Ma and Fogo, 2003). The extent of glomerular sclerosis was assessed by examining all glomeruli on a kidney cross-section and calculating the percentage involved. Tubular atrophy and interstitial fibrosis were quantified as the percentage of affected cortical parenchyma.

IF

For mouse kidney samples, Tissue-Tek O.C.T.-preserved cryosections (5 µm thick) were washed with PBS for 5 min, then left for 30 to 60 min at room temperature with blocking solution containing PBS, 2% BSA, 2% FBS, and 0.2% fish gelatin. AffiniPure fab fragment goat anti-mouse IgG (Jackson ImmunoResearch) was subsequently applied for 3 h, followed by incubation at 4°C overnight or at room temperature for 1 h with

specific primary antibodies (Table S1). Sections were then washed and incubated with the appropriate secondary antibody for 45 or 60 min at room temperature: anti-mouse IgG antibody conjugated with Alexa Fluor 594 (1:200; Thermo Fisher Scientific), anti-hamster IgG antibody conjugated with Alexa Fluor 488 (1:200; Thermo Fisher Scientific), anti-rat IgG antibody conjugated with Alexa Fluor 568 (1:500; Life Technologies), anti-rabbit IgG antibody conjugated with Alexa Fluor 594 (1:500; Life Technologies), anti-mouse IgG antibody conjugated with Alexa Fluor 594 (1:500; Jackson ImmunoResearch), and anti-goat IgG antibody conjugated with Alexa Fluor 594 (1:500; Life Technologies). Nuclei were counterstained with DAPI mounting media (ProLong Gold antifade reagent with DAPI, P36931; Invitrogen).

Antibody expression was estimated by constructing a contour mask on the bright-field image. ImageJ software (National Institutes of Health) was used to quantify DAF and C3b staining intensity.

For human kidney biopsies, Tissue-Tek O.C.T.–preserved cryosections (5 µm thick) were fixed for 10 min in acetone, and IF for polyclonal prediluted antibody anti-C3 fluorescein (FITC) conjugation was performed automatically by means of the Benchmark ultra immunostainer (Ventana Medical Systems) for 32 min. Sections were then washed three times with PBS, and the slides were mounted with glycergel (Dako).

Renal ultrastructural analysis

Fresh kidneys underwent primary fixation with 2% glutaraldehyde (Electron Microscopy Sciences) in PBS. They were then postfixed in 1% osmium tetroxide for 1 h and dehydrated in 50%, 70%, 90%, 95%, or 100% ethanol and propylene oxide for 10 min each. Samples were further infiltrated with an epoxy resin mixture. Ultrathin sections were collected on copper grids, and sections were stained using 10% uranyl acetate in 50% methanol and modified Sato lead stain. A JEOL 1011 electron microscope with a Gatan imaging system was used for picture acquisition (Pathology Laboratory, Columbia University, New York, NY). Total glomerular capillary surface area with foot process effacement were evaluated by ultrastructural analysis (more than eight glomeruli/mouse) and graded as a percentage quantification, as previously reported (Guo et al., 2008).

Urine albumin and creatinine

Urine spot samples were collected from individual mice before treatment and at weekly intervals until sacrifice. Urinary creatinine was quantified using commercial kits from Cayman Chemical. Urinary albumin was determined using a commercial assay from Bethyl Laboratories. Urinary albumin excretion was expressed as the ratio of urinary albumin to creatinine.

Cell culture

hiPod were cultured as described by Saleem et al. (2002). Redifferentiation of hiPod was performed by thermoshifting to 37°C for up to 15 d.

As indicated in the text, some experiments were repeated with human kidney progenitor cells derived from amniotic fluid (hAKPC) that were isolated and characterized as previously described (Da Sacco et al., 2013; Petrosyan et al., 2019). Briefly, hAKPC positively selected for OB-cadherin; CD24 and podocalyxin were expanded and differentiated into podocytes (hAKPC-P) by culturing on collagen I (Corning)-coated plates in VRADD media: Gibco RPMI 1640 (Thermo Fisher Scientific) supplemented with 5% FBS (Gibco), 1% antibiotic (Gibco), 1,25(OH)$_2$D$_3$ (100 nM, cholecalciferol; Sigma-Aldrich), 1 µM all-trans retinoic acid, and 100 nM dexamethasone (Sigma-Aldrich), for up to 30 d.

24-h in vitro experiments were established for hAKPC-P and hiPod (in quadruplicates). Cells were initially cultured for 24 h at a concentration of 200,000 cells per 12-well collagen I–coated plate, then incubated for 2 h in RPMI 1640 supplemented with 0.2% FBS and 1% antibiotic. After 2 h, the following groups were established and incubated for 30 min or 24 h: (1) vehicle, C3a (50 nM), or C3a + C3aR-A (50 nM); (2) LPS (5 ng/ml) + vehicle or LPS (5 ng/ml) + C3a; (3) vehicle or ADR (0.3 µg/ml; Pfizer); and (4) ADR or ADR + PLADi. Protein lysates were collected and stored at −80°C until analysis. IL-1β in the cell supernatants was measured by ELISA (R&D Systems).

12-Well chamber slides were also created for IF studies with the following culture conditions: (1) vehicle, C3a (50 nM), or C3a + C3aR-A (50 nM); (2) goat IgG (0.5 µg/ml; R&D Systems), IL-1β (50 ng/ml) + goat IgG, IL-1β + anti–IL-1β antibody (0.5 µg/ml; Gibco, Thermo Fisher Scientific), C3a (50 nM), or C3a + anti–IL-1β antibody (0.5 µg/ml; Gibco, Thermo Fisher Scientific); and (3) vehicle, ADR (0.3 µg/ml; Pfizer), vehicle + PLADi (1 µM, 1–10 phenanthroline; Sigma-Aldrich), or ADR + PLADi.

Real-time quantitative reverse transcription PCR

RNA was prepared from 0.5 cm of the mouse kidneys or from cultured hiPod using TRIzol (Invitrogen). cDNA was synthesized using reverse transcription reagent (Applied Biosystems). Real-time PCR assays using the TaqMan Universal PCR Master Mix and primer sets for human and/or mouse *DAF* (Hs00892618_m1; Mm00438377_m1), *GPLD1* (Hs00946499_m1; Mm01289339_m1), *IL1B* (Hs01555410_m1), *Rn18S* (Hs99999901_s1; Mm03928990_g1), and *GAPDH* (Hs02786624_g1; Mm99999915_g1) genes were purchased from Thermo Fisher Scientific. PCR was performed on an Applied Biosystems 7500 Fast Real-Time PCR System. All experiments were performed at least in triplicate, and gene expression was normalized to housekeeping gene *18S* or *GAPDH*.

IF studies in vitro

IF staining was performed on chamber slides of hiPod cells after 24-h incubation with components, and the results were assessed by confocal microscopy. Chamber slides were created for IF studies with the following culture conditions: C3a (50 nM), C3a + C3aR-A (50 nM), IL-1β (50 ng/ml), IL-1β + anti–IL-1β antibody (0.5 µg/ml; Gibco, Thermo Fisher Scientific), C3a (50 nM), and C3a + anti–IL-1β antibody (0.5 µg/ml; Gibco, Thermo Fisher Scientific). The chamber slides were fixed for 20 min with 4% paraformaldehyde (Santa Cruz Biotechnology) followed by serial washes with PBS. For assessment of C3a-mediated damage and rescue with anti–IL-1β, wells of interest were prepared for staining by blocking with 5% BSA (Jackson ImmunoResearch) in PBS for 30 min. Damage to podocytes was assessed by 1-h incubation at room temperature with phalloidin

(1 drop, 1,000 µl; Life Technologies) and anti-NPHS1 FITC (1:100; Life Technologies) followed by DAPI mounting (Vector Laboratories). Apoptotic podocytes were assessed by 1-h incubation at room temperature with anti–caspase-3 (1:250; Cell Signaling Technology), followed by 30-min incubation at room temperature with anti-rabbit IgG antibody conjugated with Alexa Fluor 555 (1:500; Life Technologies) and by DAPI mounting (Vector Laboratories).

Cells were visualized with a Leica Zeiss 710 microscope and analyzed using ZEN10 software. A minimum of five 20× and 40× magnification with water IF microscopic images (Leica DM5500 B microscope system) per experimental group were taken for assessment of podocyte cytoskeletal rearrangement and expression of NPHS1/nephrin and caspase-3.

Assessment of the F-actin localization was adapted from the work by Hsu et al. (2008). Briefly, the F-actin cytoskeletal reorganization for each cell was scored based on the degree of cortical F-actin ring formation, with healthy cells defined as exhibiting no cortical F-actin and injured cells exhibiting cortical F-actin on part or all of the cell border. Analysis was performed in a blinded fashion. ImageJ software was used to determine cell count.

For assessment of DAF and C3aR expression, cells were stained with anti-DAF antibody or anti-C3aR antibody (Table S1) at 4°C overnight, followed by washing and staining with secondary antibody (anti-mouse, 1:200 in blocking solution, Alexa Fluor 488; Thermo Fisher Scientific) for 1 h at room temperature. After surface staining, cells were then permeabilized with 0.1% Triton X-100/PBS (15 min) and stained for F-actin. Nuclei were counterstained with DAPI mounting media (ProLong Gold antifade reagent with DAPI; Invitrogen).

In each field, cells were segmented on the basis of actin signaling, and the intensity of DAF/C3aR normalized to the intensity of actin pixel by pixel. The mean fluorescence intensity (MFI) of the signal was then calculated for all the pixels in the cell.

Western blot (WB) analysis on hiPod

Total protein was extracted from in vitro hiPod cultures by initially washing cells with PBS, then scraping the cells with a plastic 1.8-cm blade cell scraper (Falcon Cell Scraper; Thermo Fisher Scientific) in radioimmunoprecipitation assay lysis buffer (Santa Cruz Biotechnology) or 1% SDS lysis buffer (MilliporeSigma) containing a protease inhibitor cocktail (Thermo Fisher Scientific). Protein lysates were centrifuged at 13,500 rpm and 4°C for 15 min to obtain the protein suspension. The supernatants were then collected, and protein extracts were separated on 4–20% precast Protean TGX gels (Bio-Rad Laboratories) followed by transfer onto 0.2-µm polyvinylidene fluoride membranes (Bio-Rad Laboratories) using the Trans-blot Turbo transfer system (Bio-Rad Laboratories). Membranes were soaked in methanol 100% for 5 min, quickly rinsed in 0.1% Tween-20 (Sigma-Aldrich), 1× Tris-buffered saline buffer (TBS-T). Blocking was performed in 5% nonfat dry milk (Santa Cruz Biotechnology) in TBS-T buffer for 1 h at room temperature, followed by primary antibody (NPHS1, Snail, TGF-β, or β-actin) incubation (in 2.5% milk or 5% BSA in TBS-T buffer) overnight at 4°C in rocking conditions (Table S1). Following washes in TBS-T buffer (10 min, three times), membranes were blotted with host-specific HRP-conjugated secondary antibodies diluted in 2.5% skim milk (in TBS-T) at room temperature for 30 min. Signal was detected by using the SuperSignal West Femto substrate (Thermo Fisher Scientific) and impressed on Amersham Hyperfilm ECL (GE Healthcare). Densitometry was performed on images using ImageJ software. Protein analysis of hiPod culture supernatants was performed after concentrating 10 ml of cell culture supernatant in an Amicon ultracentrifugal filter unit (MilliporeSigma) per the manufacturer's instructions. 30 µl of concentrated supernatant were run on Bolt Bis-Tris 4–12% precast gel (Thermo Fisher Scientific), then transferred and blocked as described above. Membranes were probed with anti-DAF and then with secondary antibodies, as described above (Table S1). Membranes were developed on an Odyssey Fc Imaging system (LI-COR Biosciences) and quantified using ImageStudio software (LI-COR Biosciences).

WB analysis on murine and human urine

Urine was collected and pooled from eight healthy BALB/c WT mice or eight BALB/c WT mice 2 wk after retroorbital ADR injection (10 mg/kg). Mice were aged 6–8 wk at the time of injection. Urine was concentrated using the 50K Amicon Ultra-0.5 ml centrifugal filters (Sigma-Aldrich) and stored at −80°C.

Human urine was collected from five donor samples of patients with FSGS and five healthy control individuals. Pooled urine was concentrated for 15 min at 4,000 *g* in 50K Amicon Ultra-15 ml centrifugal filters (Sigma-Aldrich). The concentrated samples were depleted of albumin using the Pierce Albumin Depletion kit (Thermo Fisher Scientific). Urine was stored at −80°C.

The urine from mouse and human samples was separated on 4–20% precast Protean TGX gels (Bio-Rad Laboratories) with recombinant mouse (55 µg/ml, 5490-CD-050; R&D Systems) or human (15 µg/ml, SRP6437; Sigma-Aldrich) CD55 protein, respectively. A total of 30 µl of each sample was loaded after preparing with Bolt LDS sample buffer and Bolt Sample Reducing Agent (Life Technologies). The gel electrophoresis was followed by transfer onto 0.2-µm polyvinylidene fluoride membranes (Bio-Rad Laboratories) using the Trans-blot Turbo transfer system (Bio-Rad Laboratories). Membranes were soaked in 100% methanol for 30 s, then quickly rinsed in 0.1% Tween-20 (Sigma-Aldrich), 1× Tris-buffered saline buffer (TBS-T). Blocking was performed in 5% nonfat dry milk (Santa Cruz Biotechnology) in TBS-T buffer for at least 1 h at room temperature, followed by primary CD55 antibody (Santa Cruz Biotechnology) overnight at 4°C in rocking conditions. Following washes in TBS-T buffer (three times for 10 min), membranes were blotted with host-specific HRP-conjugated secondary antibodies diluted in 5% BSA and 0.1% Tween-20 PBS at room temperature for 1 h. Signal was detected by using Immobilon Western HRP Substrate Peroxide Solution and Luminol Reagent (1:1; Sigma-Aldrich). Membranes were developed on an Odyssey Fc Imaging system (LI-COR Biosciences).

Cytokine analysis

Media from hiPod cultured for 24 h without and with C3a (50 nM) or C3a (50 nM) + C3aR antagonist (50 nM) were collected and stored at −80°C until used to evaluate cytokine expression in

accordance with the manufacturer's protocols. To perform cytokine measurements, samples were thawed, and protein expression profiles were obtained using a Proteome Profiler Human XL Cytokine Array Kit (R&D Systems), a membrane-based sandwich immunoassay that measures 105 human cytokines and growth factors simultaneously, following the manufacturer's protocols. Briefly, samples were incubated overnight with the nitrocellulose membranes after a blocking step, washed to remove nonspecific proteins, and biotin-labeled detection antibodies were added. The cytokine–antibody–biotin complexes were visualized using chemiluminescent detection reagents. Average chemiluminescent intensity was obtained by measuring pixel density.

Patients

We studied paraffin-embedded renal tissues of 18 patients with FSGS from the archives of the Unit of Nephrology, Dialysis and Kidney Transplant, St. Orsola Hospital, Bologna, Italy (n = 8), and from the University of Zagreb School of Medicine, Zagreb, Croatia (n = 10). Demographic and clinical parameters (proteinuria and serum creatinine levels, and glomerular filtration rate estimated by the Chronic Kidney Disease Epidemiology Collaboration equation) at the time of renal biopsy were retrieved from the hospital database.

We also analyzed frozen urine supernatants from 27 patients with FSGS obtained from the Unit of Nephrology, Dialysis and Kidney Transplant, St. Orsola Hospital, Bologna, Italy, and from the Biobank Navarrabiomed, Pamplona, Spain, integrated into the Spanish National Biobanks Network. These human samples were processed following standard operating procedures with the appropriate approval of the institutional review boards of the two institutions, and informed consent was obtained from all participants.

As controls for the histological studies, we used 10 kidney biopsies from deceased organ donors, whose biopsies were performed at the St. Orsola Hospital, to allocate them to single or double allocation on the basis of Karpinski score (Karpinski et al., 1999), in accordance with the Italian Clinical Guidelines for Organ Transplantation from Deceased Donors published by the Italian National Transplant Centre of the National Institutes of Health. Because of the retrospective nature of the study and because these samples were obtained from deceased individuals, registration or approval by the local institutional review board was waived.

C3 deposition in the glomeruli was assessed by IF on frozen sections, while DAF expression was measured by immunohistochemistry on paraffin-embedded ones. Quantification of C3 deposition and DAF expression was semiquantitative, using a scale from 0 to 3.

Statistics

We used paired or unpaired two-tailed t tests for two-group comparisons and one-way or two-way ANOVA (with Tukey test for post hoc pairwise differences) for multiple independent group comparisons. Linear regression analysis was used to test the association between urinary C3a and proteinuria in patients with FSGS. A two-tailed P value < 0.05 was regarded as statistically significant. All statistical analyses were performed using Prism, version 7, for Windows (GraphPad Software Inc.).

Study approval

Animal study protocols were approved by the institutional animal care and use committee at Icahn School of Medicine at Mount Sinai (New York, NY; IACUC number 2016-0055). Kidney tissues from patients with FSGS were obtained as deidentified leftover tissue samples from the Unit of Nephrology, Dialysis and Kidney Transplant, St. Orsola Hospital, Bologna, Italy, and from the University of Zagreb School of Medicine, Zagreb, Croatia.

Urine samples were obtained from the Unit of Nephrology, Dialysis and Kidney Transplant, St. Orsola Hospital, Bologna, Italy, and from the Biobank Navarrabiomed, Pamplona, Spain, integrated into the Spanish National Biobanks Network. All procedures were approved by the human subjects committees at the participating sites (Bologna: BO-PBMC 420/2018/Oss/AOUBo; Pamplona: Pyto2017/93), and all participants provided informed consent.

Online supplemental material

Fig. S1 shows that ADR injection associates with glomerular C3b deposition. Fig. S2 shows that podocyte-specific DAF-KO mice demonstrate increased glomerular C3b deposition in the absence of C1q or C4b deposits in response to ADR. Fig. S3 shows that mouse and hiPod express C3aR and C5aR. Table S1 lists antibodies and assay-specific concentrations.

Acknowledgments

The authors thank Kevin Kelley, PhD, and the Mouse Genetics and Gene Targeting CoRE facility at Icahn School of Medicine at Mount Sinai for production of the knockout mice. For their collaboration, we are indebted to all the participating patients, the Unit of Nephrology, Dialysis and Kidney Transplant of St. Orsola Hospital, Bologna, Italy, and the Biobank Navarrabiomed, Pamplona, Spain, integrated into the Spanish National Biobanks Network.

This work was supported by National Institutes of Health grants R01 DK119431 awarded to P. Cravedi and R01 AI132405 and R01 AI141434 awarded to P.S. Heeger. The content is solely the responsibility of the authors and does not necessarily represent the official views of the National Institutes of Health.

Author contributions: A. Angeletti, C. Cantarelli, A. Petrosyan, S. Andrighetto, K. Budge, and S. Hartzell performed most of the experiments, conducted the data analyses, and reviewed the manuscript. V.D. D'Agati scored renal mouse histology, and D. Malvi scored human histology. C. Donadei, K.N. Campbell, and J. Wong helped with podocyte cultures. J.M. Thurman and D. Galešić-Ljubanović provided biopsies from patients with FSGS and did C3d quantification. J.C. He provided assistance with the STZ-induced diabetic kidney disease model. C. Fischman measured urinary C3a in patients with FSGS. J. Manrique, G. Zaza, E. Fiaccadori, and G. La Manna helped in data interpretation and critically revised the manuscript. M. Fribourg and W. Xiao quantified DAF expression in podocytes. J. Leventhal helped with WB experiments. S. Da Sacco and L. Perin evaluated the effect of C3a on the podocyte cytoskeleton. P.S. Heeger generated the $DAF^{fl/fl}$ mice, critically helped to design the experiments and interpret the results, and reviewed/edited the manuscript. P. Cravedi conceived and oversaw the

project, designed the experiments, interpreted the results, and wrote the manuscript.

Disclosures: J.M. Thurman reported a patent to US 7,999,082 issued "Alexion Pharmaceuticals, Inc." and a patent to US 8,703,140 B2 issued "Alexion Pharmaceuticals, Inc." J. Manrique reported personal fees from Alexion Pharmaceuticals, Inc. P.S. Heeger reported personal fees from Mallinckrodt Pharmaceuticals during the conduct of the study. No other disclosures were reported.

Submitted: 10 September 2019
Revised: 28 February 2020
Accepted: 27 April 2020

References

Anders, H.J.. 2016. Of inflammasomes and alarmins: IL-1β and IL-1α in kidney disease. *J. Am. Soc. Nephrol.* 27:2564–2575. https://doi.org/10.1681/ASN.2016020177

Angeletti, A., M. Marasà, and P. Cravedi. 2017. CD55 deficiency and protein-losing enteropathy [letter]. *N. Engl. J. Med.* 377:1499–1500. https://doi.org/10.1056/NEJMc1710011

Asano, T., F. Niimura, I. Pastan, A.B. Fogo, I. Ichikawa, and T. Matsusaka. 2005. Permanent genetic tagging of podocytes: fate of injured podocytes in a mouse model of glomerular sclerosis. *J. Am. Soc. Nephrol.* 16: 2257–2262. https://doi.org/10.1681/ASN.2004121134

Asgari, E., G. Le Friec, H. Yamamoto, E. Perucha, S.S. Sacks, J. Köhl, H.T. Cook, and C. Kemper. 2013. C3a modulates IL-1β secretion in human monocytes by regulating ATP efflux and subsequent NLRP3 inflammasome activation. *Blood.* 122:3473–3481. https://doi.org/10.1182/blood-2013-05-502229

Bao, L., M. Haas, J. Pippin, Y. Wang, T. Miwa, A. Chang, A.W. Minto, M. Petkova, G. Qiao, W.C. Song, et al. 2009. Focal and segmental glomerulosclerosis induced in mice lacking decay-accelerating factor in T cells. *J. Clin. Invest.* 119:1264–1274. https://doi.org/10.1172/JCI36000

Boehm, M., E.N. Bukosza, N. Huttary, R. Herzog, C. Aufricht, K. Kratochwill, and C.A. Gebeshuber. 2019. A systems pharmacology workflow with experimental validation to assess the potential of anakinra for treatment of focal and segmental glomerulosclerosis. *PLoS One.* 14. e0214332. https://doi.org/10.1371/journal.pone.0214332

Breyer, M.D., E. Böttinger, F.C. Brosius, III, T.M. Coffman, R.C. Harris, C.W. Heilig, and K. Sharma; AMDCC. 2005. Mouse models of diabetic nephropathy. *J. Am. Soc. Nephrol.* 16:27–45. https://doi.org/10.1681/ASN.2004080648

Bus, P., J.S. Chua, C.Q.F. Klessens, M. Zandbergen, R. Wolterbeek, C. van Kooten, L.A. Trouw, J.A. Bruijn, and H.J. Baelde. 2018. Complement activation in patients with diabetic nephropathy. *Kidney Int. Rep.* 3: 302–313. https://doi.org/10.1016/j.ekir.2017.10.005

Chen, A., L.F. Sheu, Y.S. Ho, Y.F. Lin, W.Y. Chou, T.C. Chou, and W.H. Lee. 1998. Experimental focal segmental glomerulosclerosis in mice. *Nephron.* 78:440–452. https://doi.org/10.1159/000044974

Coffelt, S.B., K. Kersten, C.W. Doornebal, J. Weiden, K. Vrijland, C.S. Hau, N.J.M. Verstegen, M. Ciampricotti, L.J.A.C. Hawinkels, J. Jonkers, et al. 2015. IL-17-producing γδ T cells and neutrophils conspire to promote breast cancer metastasis. *Nature.* 522:345–348. https://doi.org/10.1038/nature14282

Cravedi, P., and P.S. Heeger. 2014. Complement as a multifaceted modulator of kidney transplant injury. *J. Clin. Invest.* 124:2348–2354. https://doi.org/10.1172/JCI72273

Cravedi, P., J.B. Kopp, and G. Remuzzi. 2013a. Recent progress in the pathophysiology and treatment of FSGS recurrence. *Am. J. Transplant.* 13: 266–274. https://doi.org/10.1111/ajt.12045

Cravedi, P., J. Leventhal, P. Lakhani, S.C. Ward, M.J. Donovan, and P.S. Heeger. 2013b. Immune cell-derived C3a and C5a costimulate human T cell alloimmunity. *Am. J. Transplant.* 13:2530–2539. https://doi.org/10.1111/ajt.12405

Da Sacco, S., S. Sedrakyan, F. Boldrin, S. Giuliani, P. Parnigotto, R. Habibian, D. Warburton, R.E. De Filippo, and L. Perin. 2010. Human amniotic fluid as a potential new source of organ specific precursor cells for future regenerative medicine applications. *J. Urol.* 183:1193–1200. https://doi.org/10.1016/j.juro.2009.11.006

Da Sacco, S., K.V. Lemley, S. Sedrakyan, I. Zanusso, A. Petrosyan, J. Peti-Peterdi, J. Burford, R.E. De Filippo, and L. Perin. 2013. A novel source of cultured podocytes. *PLoS One.* 8. e81812. https://doi.org/10.1371/journal.pone.0081812

Davitz, M.A., J. Hom, and S. Schenkman. 1989. Purification of a glycosylphosphatidylinositol-specific phospholipase D from human plasma. *J. Biol. Chem.* 264:13760–13764.

Dho, S.H., J.C. Lim, and L.K. Kim. 2018. Beyond the role of CD55 as a complement component. *Immune Netw.* 18. e11. https://doi.org/10.4110/in.2018.18.e11

Dinarello, C.A., A. Simon, and J.W. van der Meer. 2012. Treating inflammation by blocking interleukin-1 in a broad spectrum of diseases. *Nat. Rev. Drug Discov.* 11:633–652. https://doi.org/10.1038/nrd3800

Duann, P., P.H. Lin, and E.A. Lianos. 2019. Data on characterization of metalloporphyrin-mediated HO-1 and DAF induction in rat glomeruli and podocytes. *Data Brief.* 22:279–285. https://doi.org/10.1016/j.dib.2018.11.108

Flyvbjerg, A.. 2017. The role of the complement system in diabetic nephropathy. *Nat. Rev. Nephrol.* 13:311–318. https://doi.org/10.1038/nrneph.2017.31

Frohman, M.A.. 2015. The phospholipase D superfamily as therapeutic targets. *Trends Pharmacol. Sci.* 36:137–144. https://doi.org/10.1016/j.tips.2015.01.001

Garovic, V.D., and P. August. 2016. Sex differences and renal protection: Keeping in touch with your feminine side. *J. Am. Soc. Nephrol.* 27: 2921–2924. https://doi.org/10.1681/ASN.2016040454

Gephardt, G.N., R.R. Tubbs, K.L. Popowniak, and J.T. McMahon. 1986. Focal and segmental glomerulosclerosis: Immunohistologic study of 20 renal biopsy specimens. *Arch. Pathol. Lab. Med.* 110:902–905.

Guo, J., R. Ananthakrishnan, W. Qu, Y. Lu, N. Reiniger, S. Zeng, W. Ma, R. Rosario, S.F. Yan, R. Ramasamy, et al. 2008. RAGE mediates podocyte injury in adriamycin-induced glomerulosclerosis. *J. Am. Soc. Nephrol.* 19: 961–972. https://doi.org/10.1681/ASN.2007101109

Habib, R., E. Girardin, M.F. Gagnadoux, N. Hinglais, M. Levy, and M. Broyer. 1988. Immunopathological findings in idiopathic nephrosis: clinical significance of glomerular "immune deposits.". *Pediatr. Nephrol.* 2: 402–408. https://doi.org/10.1007/BF00853431

Haeffner-Cavaillon, N., J.M. Cavaillon, M. Laude, and M.D. Kazatchkine. 1987. C3a(C3adesArg) induces production and release of interleukin 1 by cultured human monocytes. *J. Immunol.* 139:794–799.

Heeger, P.S., P.N. Lalli, F. Lin, A. Valujskikh, J. Liu, N. Muqim, Y. Xu, and M.E. Medof. 2005. Decay-accelerating factor modulates induction of T cell immunity. *J. Exp. Med.* 201:1523–1530. https://doi.org/10.1084/jem.20041967

Hsu, H.H., S. Hoffmann, N. Endlich, A. Velic, A. Schwab, T. Weide, E. Schlatter, and H. Pavenstädt. 2008. Mechanisms of angiotensin II signaling on cytoskeleton of podocytes. *J. Mol. Med. (Berl.).* 86:1379–1394. https://doi.org/10.1007/s00109-008-0399-y

Ju, W., C.S. Greene, F. Eichinger, V. Nair, J.B. Hodgin, M. Bitzer, Y.S. Lee, Q. Zhu, M. Kehata, M. Li, et al. 2013. Defining cell-type specificity at the transcriptional level in human disease. *Genome Res.* 23:1862–1873. https://doi.org/10.1101/gr.155697.113

Karpinski, J., G. Lajoie, D. Cattran, S. Fenton, J. Zaltzman, C. Cardella, and E. Cole. 1999. Outcome of kidney transplantation from high-risk donors is determined by both structure and function. *Transplantation.* 67: 1162–1167. https://doi.org/10.1097/00007890-199904270-00013

Kitiyakara, C., P. Eggers, and J.B. Kopp. 2004. Twenty-one-year trend in ESRD due to focal segmental glomerulosclerosis in the United States. *Am. J. Kidney Dis.* 44:815–825. https://doi.org/10.1016/S0272-6386(04)01081-9

Kurolap, A., O. Eshach-Adiv, and H.N. Baris. 2017. CD55 deficiency and protein-losing enteropathy [letter]. *N. Engl. J. Med.* 377:1500. https://doi.org/10.1056/NEJMc1707173

Lenderink, A.M., K. Liegel, D. Ljubanović, K.E. Coleman, G.S. Gilkeson, V.M. Holers, and J.M. Thurman. 2007. The alternative pathway of complement is activated in the glomeruli and tubulointerstitium of mice with adriamycin nephropathy. *Am. J. Physiol. Renal Physiol.* 293:F555–F564. https://doi.org/10.1152/ajprenal.00403.2006

Li, L., Q. Yin, X. Tang, L. Bai, J. Zhang, S. Gou, H. Zhu, J. Cheng, P. Fu, and F. Liu. 2014. C3a receptor antagonist ameliorates inflammatory and fibrotic signals in type 2 diabetic nephropathy by suppressing the activation of TGF-β/smad3 and IKBα pathway. *PLoS One.* 9. e113639. https://doi.org/10.1371/journal.pone.0113639

Liu, J., J. Xie, X. Zhang, J. Tong, X. Hao, H. Ren, W. Wang, and N. Chen. 2017. Serum C3 and renal outcome in patients with primary focal segmental glomerulosclerosis. *Sci. Rep.* 7:4095. https://doi.org/10.1038/s41598-017-03344-1

Ma, L.J., and A.B. Fogo. 2003. Model of robust induction of glomerulosclerosis in mice: importance of genetic background. *Kidney Int.* 64:350–355. https://doi.org/10.1046/j.1523-1755.2003.00058.x

Macconi, D., M. Abbate, M. Morigi, S. Angioletti, M. Mister, S. Buelli, M. Bonomelli, P. Mundel, K. Endlich, A. Remuzzi, et al. 2006. Permselective dysfunction of podocyte-podocyte contact upon angiotensin II unravels the molecular target for renoprotective intervention. *Am. J. Pathol.* 168:1073–1085. https://doi.org/10.2353/ajpath.2006.050701

Mathern, D.R., and P.S. Heeger. 2015. Molecules great and small: The complement system. *Clin. J. Am. Soc. Nephrol.* 10:1636–1650. https://doi.org/10.2215/CJN.06230614

Matsui, I., T. Ito, H. Kurihara, E. Imai, T. Ogihara, and M. Hori. 2007. Snail, a transcriptional regulator, represses nephrin expression in glomerular epithelial cells of nephrotic rats. *Lab. Invest.* 87:273–283. https://doi.org/10.1038/labinvest.3700518

Matsusaka, T., J. Xin, S. Niwa, K. Kobayashi, A. Akatsuka, H. Hashizume, Q.C. Wang, I. Pastan, A.B. Fogo, and I. Ichikawa. 2005. Genetic engineering of glomerular sclerosis in the mouse via control of onset and severity of podocyte-specific injury. *J. Am. Soc. Nephrol.* 16:1013–1023. https://doi.org/10.1681/ASN.2004080720

Medof, M.E., T. Kinoshita, and V. Nussenzweig. 1984. Inhibition of complement activation on the surface of cells after incorporation of decay-accelerating factor (DAF) into their membranes. *J. Exp. Med.* 160:1558–1578. https://doi.org/10.1084/jem.160.5.1558

Medof, M.E., E.I. Walter, J.L. Rutgers, D.M. Knowles, and V. Nussenzweig. 1987. Identification of the complement decay-accelerating factor (DAF) on epithelium and glandular cells and in body fluids. *J. Exp. Med.* 165:848–864. https://doi.org/10.1084/jem.165.3.848

Morigi, M., M. Locatelli, C. Rota, S. Buelli, D. Corna, P. Rizzo, M. Abbate, D. Conti, L. Perico, L. Longaretti, et al. 2016. A previously unrecognized role of C3a in proteinuric progressive nephropathy. *Sci. Rep.* 6:28445. https://doi.org/10.1038/srep28445

Niemir, Z.I., H. Stein, G. Dworacki, P. Mundel, N. Koehl, B. Koch, F. Autschbach, K. Andrassy, E. Ritz, R. Waldherr, et al. 1997. Podocytes are the major source of IL-1 alpha and IL-1 beta in human glomerulonephritides. *Kidney Int.* 52:393–403. https://doi.org/10.1038/ki.1997.346

Ozen, A., W.A. Comrie, and M.J. Lenardo. 2017. CD55 deficiency and protein-losing enteropathy [letter]. *N. Engl. J. Med.* 377:1499–1500. https://doi.org/10.1056/NEJMoa1615887

Packard, B.D., and J.M. Weiler. 1983. Steroids inhibit activation of the alternative-amplification pathway of complement. *Infect. Immun.* 40:1011–1014. https://doi.org/10.1128/IAI.40.3.1011-1014.1983

Papeta, N., Z. Zheng, E.A. Schon, S. Brosel, M.M. Altintas, S.H. Nasr, J. Reiser, V.D. D'Agati, and A.G. Gharavi. 2010. Prkdc participates in mitochondrial genome maintenance and prevents Adriamycin-induced nephropathy in mice. *J. Clin. Invest.* 120:4055–4064. https://doi.org/10.1172/JCI43721

Petrosyan, A., P. Cravedi, V. Villani, A. Angeletti, J. Manrique, A. Renieri, R.E. De Filippo, L. Perin, and S. Da Sacco. 2019. A glomerulus-on-a-chip to recapitulate the human glomerular filtration barrier. *Nat. Commun.* 10:3656. https://doi.org/10.1038/s41467-019-11577-z

Pippin, J.W., P.T. Brinkkoetter, F.C. Cormack-Aboud, R.V. Durvasula, P.V. Hauser, J. Kowalewska, R.D. Krofft, C.M. Logar, C.B. Marshall, T. Ohse, et al. 2009. Inducible rodent models of acquired podocyte diseases. *Am. J. Physiol. Renal Physiol.* 296:F213–F229. https://doi.org/10.1152/ajprenal.90421.2008

Pollak, M.R.. 2002. Inherited podocytopathies: FSGS and nephrotic syndrome from a genetic viewpoint. *J. Am. Soc. Nephrol.* 13:3016–3023. https://doi.org/10.1097/01.ASN.0000039569.34360.5E

Raedler, H., M. Yang, P.N. Lalli, M.E. Medof, and P.S. Heeger. 2009. Primed $CD8^+$ T-cell responses to allogeneic endothelial cells are controlled by local complement activation. *Am. J. Transplant.* 9:1784–1795. https://doi.org/10.1111/j.1600-6143.2009.02723.x

Sakemi, T., N. Ohtsuka, Y. Tomiyoshi, and F. Morito. 1996. Sex difference in progression of adriamycin-induced nephropathy in rats. *Am. J. Nephrol.* 16:540–547. https://doi.org/10.1159/000169057

Saleem, M.A., M.J. O'Hare, J. Reiser, R.J. Coward, C.D. Inward, T. Farren, C.Y. Xing, L. Ni, P.W. Mathieson, and P. Mundel. 2002. A conditionally immortalized human podocyte cell line demonstrating nephrin and podocin expression. *J. Am. Soc. Nephrol.* 13:630–638.

Schlondorff, J.. 2008. Nephrin AKTs on actin: The slit diaphragm–actin cytoskeleton signaling network expands. *Kidney Int.* 73:524–526. https://doi.org/10.1038/sj.ki.5002741

Servais, A., L.H. Noël, L.T. Roumenina, M. Le Quintrec, S. Ngo, M.A. Dragon-Durey, M.A. Macher, J. Zuber, A. Karras, F. Provot, et al. 2012. Acquired and genetic complement abnormalities play a critical role in dense deposit disease and other C3 glomerulopathies. *Kidney Int.* 82:454–464. https://doi.org/10.1038/ki.2012.63

Sethi, S., C.M. Nester, and R.J. Smith. 2012. Membranoproliferative glomerulonephritis and C3 glomerulopathy: resolving the confusion. *Kidney Int.* 81:434–441. https://doi.org/10.1038/ki.2011.399

Sheen, J.H., M.G. Strainic, J. Liu, W. Zhang, Z. Yi, M.E. Medof, and P.S. Heeger. 2017. TLR-induced murine dendritic cell (DC) activation requires DC-intrinsic complement. *J. Immunol.* 199:278–291. https://doi.org/10.4049/jimmunol.1700339

Smith, R.J.H., G.B. Appel, A.M. Blom, H.T. Cook, V.D. D'Agati, F. Fakhouri, V. Fremeaux-Bacchi, M. Józsi, D. Kavanagh, J.D. Lambris, et al. 2019. C3 glomerulopathy — understanding a rare complement-driven renal disease. *Nat. Rev. Nephrol.* 15:129–143. https://doi.org/10.1038/s41581-018-0107-2

Sutterwala, F.S., S. Haasken, and S.L. Cassel. 2014. Mechanism of NLRP3 inflammasome activation. *Ann. N. Y. Acad. Sci.* 1319:82–95. https://doi.org/10.1111/nyas.12458

Takano, Y., K. Yamauchi, K. Hayakawa, N. Hiramatsu, A. Kasai, M. Okamura, M. Yokouchi, A. Shitamura, J. Yao, and M. Kitamura. 2007. Transcriptional suppression of nephrin in podocytes by macrophages: roles of inflammatory cytokines and involvement of the PI3K/Akt pathway. *FEBS Lett.* 581:421–426. https://doi.org/10.1016/j.febslet.2006.12.051

Thurman, J.M., M. Wong, B. Renner, A. Frazer-Abel, P.C. Giclas, M.S. Joy, D. Jalal, M.K. Radeva, J. Gassman, D.S. Gipson, et al. 2015. Complement activation in patients with focal segmental glomerulosclerosis. *PLoS One.* 10. e0136558. https://doi.org/10.1371/journal.pone.0136558

Turnberg, D., M. Lewis, J. Moss, Y. Xu, M. Botto, and H.T. Cook. 2006. Complement activation contributes to both glomerular and tubulointerstitial damage in adriamycin nephropathy in mice. *J. Immunol.* 177:4094–4102. https://doi.org/10.4049/jimmunol.177.6.4094

Varan, Ö., H. Kucuk, H. Babaoglu, S.C. Guven, M.A. Ozturk, S. Haznedaroglu, B. Goker, and A. Tufan. 2019. Efficacy and safety of interleukin-1 inhibitors in familial Mediterranean fever patients complicated with amyloidosis. *Mod. Rheumatol.* 29:363–366. https://doi.org/10.1080/14397595.2018.1457469

Wang, Y., Y.P. Wang, Y.-C. Tay, and D.C.H. Harris. 2000. Progressive adriamycin nephropathy in mice: sequence of histologic and immunohistochemical events. *Kidney Int.* 58:1797–1804. https://doi.org/10.1046/j.1523-1755.2000.00342.x

Wharram, B.L., M. Goyal, J.E. Wiggins, S.K. Sanden, S. Hussain, W.E. Filipiak, T.L. Saunders, R.C. Dysko, K. Kohno, L.B. Holzman, et al. 2005. Podocyte depletion causes glomerulosclerosis: diphtheria toxin-induced podocyte depletion in rats expressing human diphtheria toxin receptor transgene. *J. Am. Soc. Nephrol.* 16:2941–2952. https://doi.org/10.1681/ASN.2005010055

Wong, A.K., A. Krishnan, and O.G. Troyanskaya. 2018. GIANT 2.0: genome-scale integrated analysis of gene networks in tissues. *Nucleic Acids Res.* 46(W1):W65–W70. https://doi.org/10.1093/nar/gky408

Wu, C., and S. Dedhar. 2001. Integrin-linked kinase (ILK) and its interactors: a new paradigm for the coupling of extracellular matrix to actin cytoskeleton and signaling complexes. *J. Cell Biol.* 155:505–510. https://doi.org/10.1083/jcb.200108077

Yan, J., Y. Li, H. Yang, L. Zhang, B. Yang, M. Wang, and Q. Li. 2018. Interleukin-17A participates in podocyte injury by inducing IL-1β secretion through ROS-NLRP3 inflammasome-caspase-1 pathway. *Scand. J. Immunol.* 87. e12645. https://doi.org/10.1111/sji.12645

Yang, J.W., A.K. Dettmar, A. Kronbichler, H.Y. Gee, M. Saleem, S.H. Kim, and J.I. Shin. 2018. Recent advances of animal model of focal segmental glomerulosclerosis. *Clin. Exp. Nephrol.* 22:752–763. https://doi.org/10.1007/s10157-018-1552-8

Zhang, Y.M., Q.H. Gu, J. Huang, Z. Qu, X. Wang, L.Q. Meng, F. Wang, G. Liu, Z. Cui, and M.H. Zhao. 2016. Clinical significance of IgM and C3 glomerular deposition in primary focal segmental glomerulosclerosis. *Clin. J. Am. Soc. Nephrol.* 11:1582–1589. https://doi.org/10.2215/CJN.01190216

Zhao, L., X. Wang, L. Sun, H. Nie, X. Liu, Z. Chen, and G. Guan. 2016. Critical role of serum response factor in podocyte epithelial-mesenchymal transition of diabetic nephropathy. *Diab. Vasc. Dis. Res.* 13:81–92. https://doi.org/10.1177/1479164115588545

Zheng, Z., K.M. Schmidt-Ott, S. Chua, K.A. Foster, R.Z. Frankel, P. Pavlidis, J. Barasch, V.D. D'Agati, and A.G. Gharavi. 2005. A Mendelian locus on chromosome 16 determines susceptibility to doxorubicin nephropathy in the mouse. *Proc. Natl. Acad. Sci. USA.* 102:2502–2507. https://doi.org/10.1073/pnas.0409786102

Zheng, Z., P. Pavlidis, S. Chua, V.D. D'Agati, and A.G. Gharavi. 2006. An ancestral haplotype defines susceptibility to doxorubicin nephropathy in the laboratory mouse. *J. Am. Soc. Nephrol.* 17:1796–1800. https://doi.org/10.1681/ASN.2005121373

JEM

Supplemental material

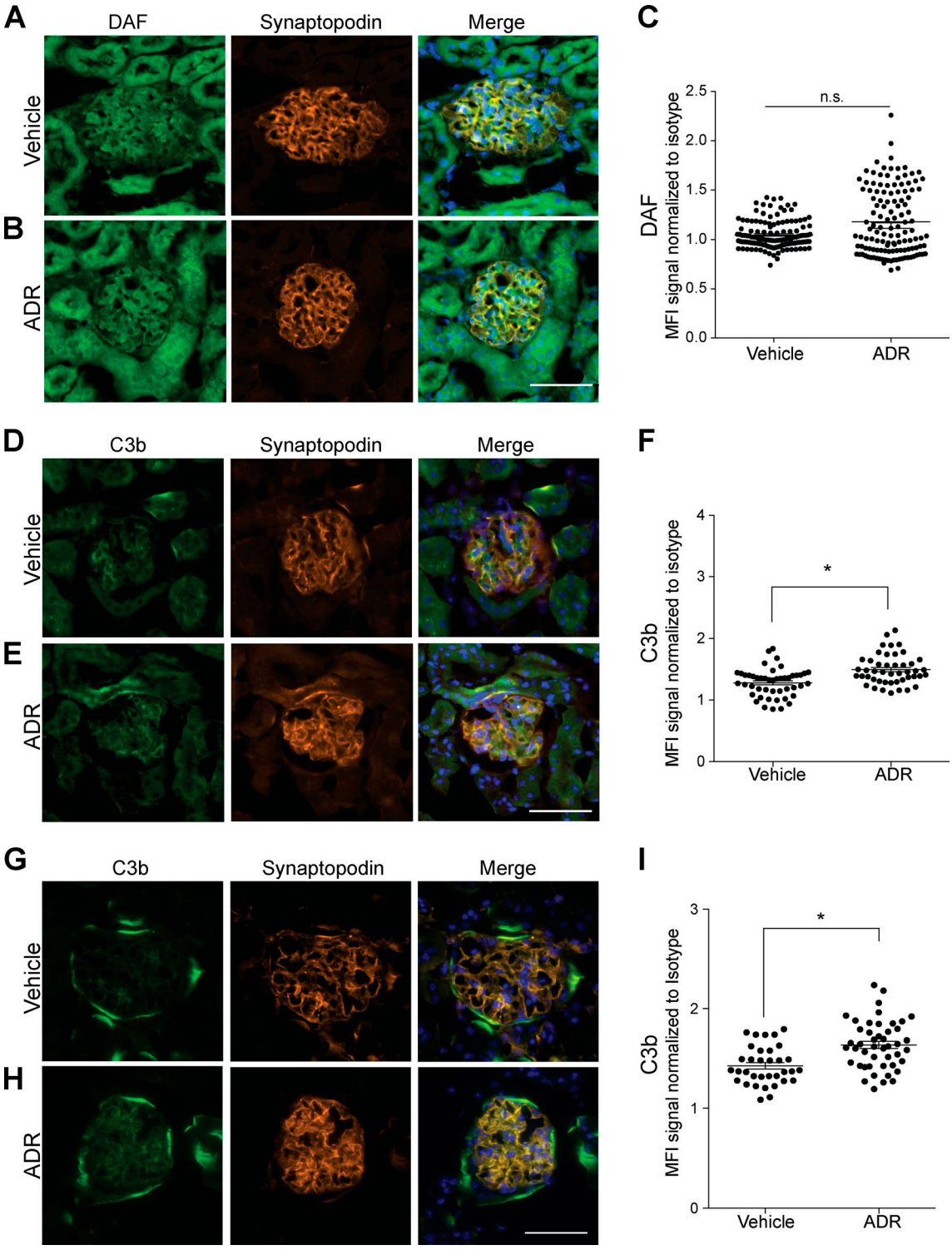

Figure S1. **ADR injection associates with glomerular C3b deposition. (A–F)** Representative pictures of glomerular DAF (A and B) and C3b staining (D and E) and data quantification (C and F) of male B6 WT mice at 2 wk after treatment with vehicle or ADR (20 mg/kg, i.v., *n* = 4). **(G–I)** Representative glomerular C3b deposition (G and H) and data quantification (I) in kidneys from B6 DAF$^{-/-}$ mice at 2 wk after ADR or vehicle injection (*n* = 4). All images within the same experiment, including vehicle and ADR, were captured at the same exposure time. n.s., not significant. Scale bars: 50 µm. *P < 0.05. Error bars are SEM.

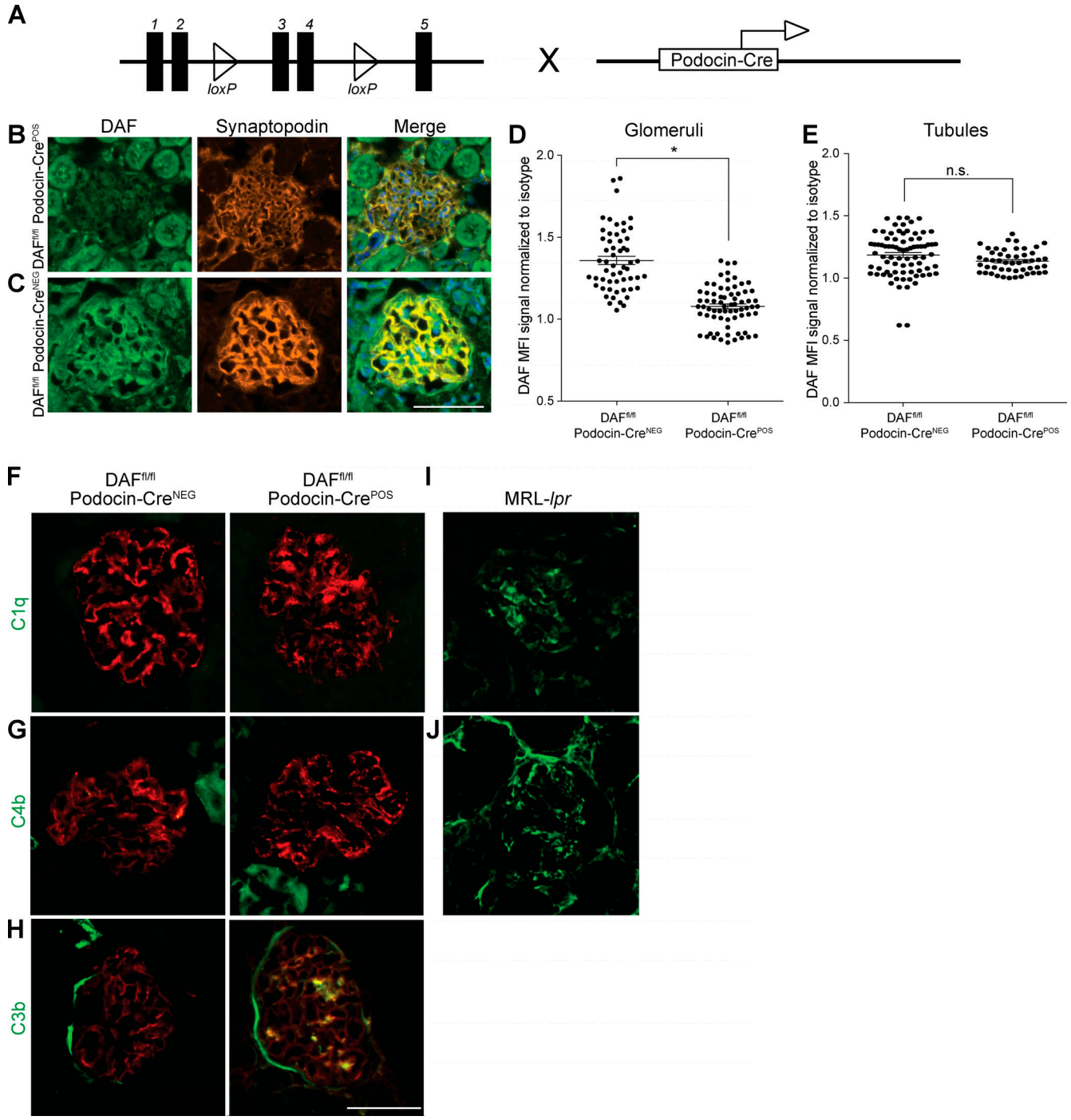

Figure S2. **Podocyte-specific DAF-KO mice show increased glomerular C3b deposition in the absence of C1q or C4b deposits in response to ADR. (A)** Schematic demonstrating the breeding of the DAF$^{fl/fl}$ mice with the podocin-Cre mice to generate DAF$^{fl/fl}$ podocin-Cre^{POS} animals. **(B–E)** Representative pictures of renal staining of DAF expression in the glomeruli and tubules (B and C) and data quantification (D and E) from 8-wk-old male DAF$^{fl/fl}$ podocin-Cre^{POS} and podocin-Cre^{NEG} mice. DAF glomerular and tubular fluorescence intensity were quantified as in Fig. 1. **(F–J)** Representative glomerular C1q (F), C4 (G), and C3b (H) staining in B6 DAF$^{fl/fl}$ podocin-Cre^{NEG} and podocin-Cre^{POS} mice at 2 wk after ADR injection. Synaptopodin is stained in red. As positive controls for C1q and C4b, we used MRL-*lpr* lupus-prone mice at 4 mo of age (I and J). All experimental data were verified in at least three independent experiments. n.s., not significant. Scale bars: 50 µm. *P < 0.05. Error bars are SEM.

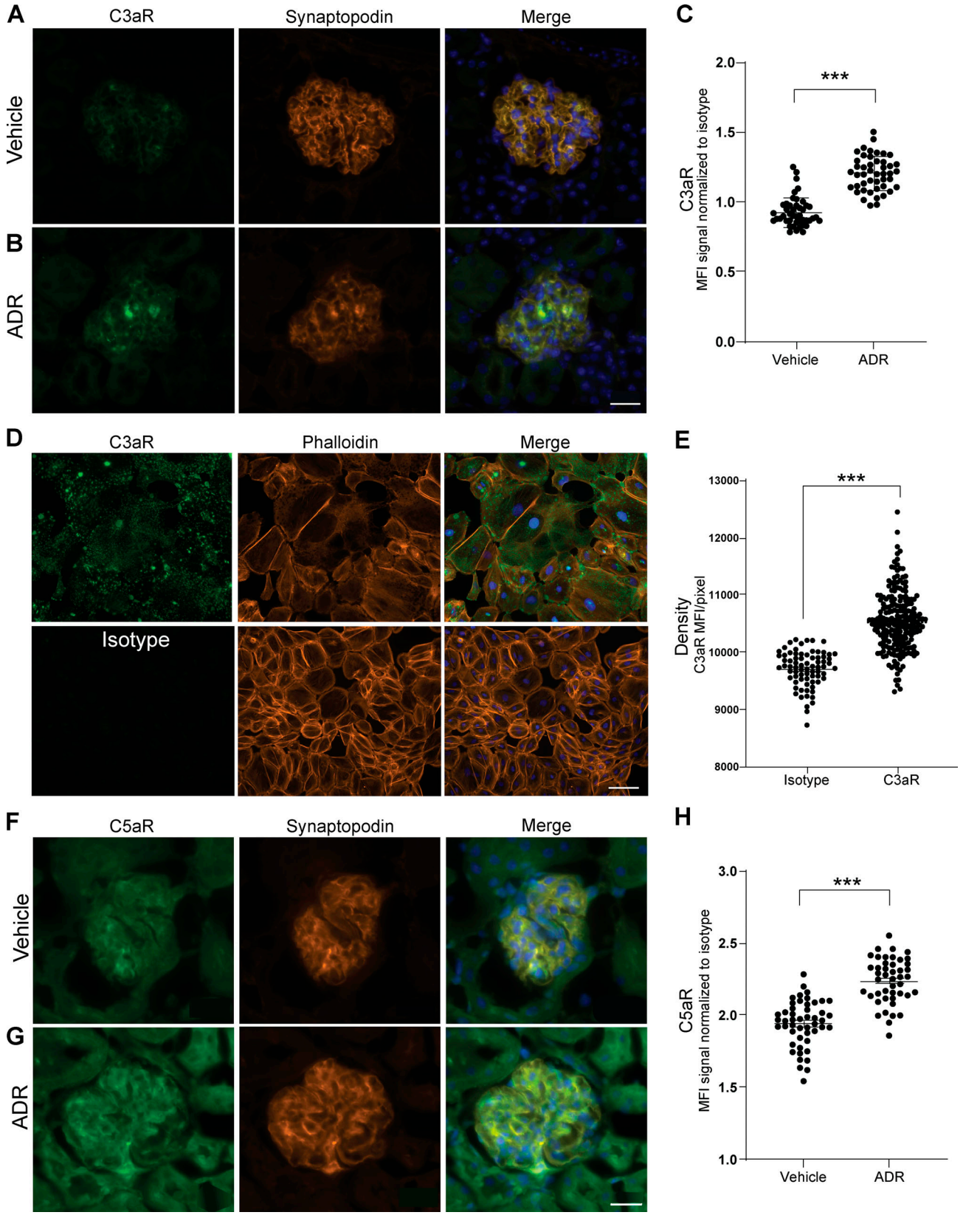

Figure S3. **Mouse and immortalized human podocytes express C3aR and C5aR. (A–C)** Representative pictures of glomerular C3aR (A and B) and data quantification (C) of male WT BALB/c mice at 2 wk after treatment with vehicle or ADR (10 mg/kg, i.v., *n* = 4). Scale bars: 20 µm. **(D and E)** Representative images (D) and densitometric analysis (E) of C3aR expression over isotype in hiPod. Scale bars: 100 µm. All experimental data were verified in at least three independent experiments. **(F–H)** Representative pictures of glomerular C5aR (F and G) and data quantification (H) of male WT BALB/c mice at 2 wk after treatment with vehicle or ADR (*n* = 4). Scale bars: 20 µm. ***P < 0.001. Error bars are SEM.

Table S1 is provided online and lists antibodies and assay-specific concentrations.